Pure Appl. Geophys. 183 (2026), 1579–1606

https://doi.org/10.1007/s00024-026-03928-x

Pure and Applied Geophysics

A Stochastic Model for Earthquake Rupture

Tsung-Hsi Wu[1] and Chien-Chih Chen[1,2]

Abstract—Analytical solutions for the dynamics of asymmetric many-body systems are impractical to obtain, and numerical solutions usually exhibit chaotic behavior if interactions between bodies are considered. To address these challenges, stochastic approaches have been widely employed in modelling many-body systems. Following Langevin's approach, we propose a stochastic dynamic model for the earthquake rupture process, in which complexity in degrees of freedom is reduced by introducing a random force that accounts for uncertainties in faulting plane heterogeneity and structural collisions. In this coarse-grained framework, the random term captures unresolved heterogeneity and interactions at a macroscopic system scale; it does not assert that rupture at the scale of specific fault patches is inherently random. Under this approach, treating the tectonic process as a Coulomb friction process allows the proposed Langevin equation to be viewed as a stochastic variant of Newton's second law, thereby attributing physical significance to the equation through the realization of stochastic processes as sample paths. This study analyzes synthetic events generated numerically with the Langevin equation to determine the energy–duration relationship and solves the corresponding Fokker–Planck equation to obtain the theoretical rupture slip distribution. The results for the energy–duration relationship show a consistent scaling law within our additive-noise, Coulomb-damping framework, with the scaling exponent varying under different slip velocity thresholds used to define synthetic events. Regarding the slip distribution, solutions obtained assuming relatively large external driving forces align closely with the truncated exponential model, characterizing rupture models of large earthquake events worldwide. The proposed Langevin equation provides a physical basis that offers insights into the scaling parameter of such laws and suggests a connection between the scaling parameter and the dissipative and environmental noise effects of the faulting system.

Keywords: Earthquake rupture, friction process, stochastic dynamics, Langevin equation, Fokker–Planck equation.

1. Introduction

Stick–slip frictional instabilities are fracture-like phenomena occurring on non-uniform prestressed interfaces (Albertini et al., 2020); under this framework, earthquakes can be realized as stick–slip events in a frictional process of a tectonic scale. The stick–slip explanation of earthquakes can be dated back to Brace and Byerlee (1966), who considered earthquakes as transitory phenomena subject to long-term friction within the Earth's crust.

Friction, specifically Coulomb friction, arises from interactions between geometric structures on contacting interfaces (Scholz, 1990). Haessig and Friedland (1991) further conceptualized Coulomb friction as a macroscopic phenomenon comprising successive and repetitive stick–slip events. The notion of stick–slip is analogous in the context of Coulomb friction and earthquakes, representing the physical bonding and bonding failure under stressed conditions. In seismology, bonding refers to interlocking between surfaces, while bonding failure corresponds to the breakdown of interlocked asperities. Due to this similarity, laboratory experiments on Coulomb friction have been extensively employed to study earthquake physics, as they exhibit stick–slips resembling earthquakes on a smaller scale (Kaproth & Marone, 2013; Brace & Byerlee, 1966; Ruina, 1983; Okubo & Dieterich, 1984; Adjemian & Evesque, 2004; Vargas et al., 2008; Ohnaka et al., 1986; Moreno-Torres et al., 2018). Similar to earthquakes, complex and chaotic behavior is often observed in laboratory-scale Coulomb friction processes. To represent realistic contact conditions, stochastic process or fractal surface models had been commonly applied in the simulation of friction processes (Wojewoda et al., 2008; Pei et al., 2005).

[1] Department of Earth Sciences, National Central University, Zongda Road, Taoyuan 32001, Taiwan. E-mail: okatsn@gmail.com; chienchih.chen@g.ncu.edu.tw
[2] Earthquake-Disaster and Risk Evaluation and Management Center, National Central University, Zongda Road, Taoyuan 32001, Taiwan.

Despite the inherent inaccessibility of critical material or frictional strengths, slip nucleation in earthquakes shares fundamental mechanisms with laboratory stick–slip frictional processes. The complexity of earthquake phenomena is a critical key point highlighted in seismology. Earthquake rupture is in general suggested occurring within a spatially heterogeneous stress and strength environment (Rivera & Kanamori, 2002), involving a combination of frictional slip instability and rock fracture (Ohnaka et al., 1997). Considering the scale and the basically uncountable number of degrees of freedom, obtaining analytical molecular dynamics solutions for the interactions between the physical bodies composing a faulting system is impossible (Rundle et al., 2003). On the other hand, scaling laws, such as the relationship between seismic moment and fault size, seismic moment and rupture duration, and the distribution of earthquake magnitudes (Gutenberg-Richter law), have been extensively validated (Scholz & Aviles, 1986; Carpinteri & Paggi, 2009; Goebel et al., 2015; Geller, 1976; Legrand, 2002; Wang, 2019). These scaling laws suggest that earthquakes share similar fundamental mechanisms regardless of their scale, and this scaling invariance indicates a self-similar nature of earthquakes where spatiotemporal correlations are unified across all scales (Bak et al., 2002).

Self-similarity is a property related to fractality; in seismology, both concepts involve the repetition of patterns at different scales that summarize the complexity of the earthquake. A self-similar process is a type of stochastic process where the statistical properties based on measurements of different scales remain invariant. In the context of earthquake rupture, consistent self-similarity are observed from laboratory to field, and manifests in various faulting properties (Brown & Scholz, 1985a, b; Renard & Candela, 2017; Kagan, 1997; Aviles et al., 1987; Velde et al., 1991; Aki, 1987). Empirical scaling laws obtained from this kind of observations not only provide fundamental insights into the nature of earthquake ruptures, but also serve as a basis for developing models and conducting simulations. In many studies, slip/stress distributions, ground motion, and fault surface geometries are assumed to be stochastic, aiming to create more realistic rupture models and facilitate improved estimation or prediction (Lavallee et al., 2006; Mai & Beroza, 2002; Murphy & Herrero, 2020; Sun et al., 2018; Tsai & Hirth, 2020). Additionally, high-frequency ground motions are very likely to be attributed more to the collision of structures during the friction process rather than abrupt slips (Tsai & Hirth, 2020). These indications collectively support the conclusion that the general earthquake rupture process is a dissipative stochastic process.

The study of stochastic processes was initiated by Einstein in 1905, when he successfully modeled the dynamics of Brownian particles using the kinetic theory of heat (Einstein, 2003; Renn, 2005). Einstein's approach, known as the Fokker-Planck equation (FPE), provides the probability density function (PDF) of particle velocity. On the other hand, Langevin, in 1908, introduced the Langevin equation to describe Brownian motion (Hanggi & Marchesoni, 2005). By incorporating the effect of the random environment into a single noise term, Langevin's approach effectively reduces the number of degrees of freedom in the equation of motion, making solving the problem feasible.

In our study, we model the aggregate rupture dynamics using a coarse-grained stochastic friction framework with deterministic external and stochastic internal sources providing the momentum for the rupture to propagate. Inspired by the Brownian motion, we explore the capability of applying Langevin's approach to obtain statistical properties and theoretical scaling laws in seismology. The idea is simple: we consider the seismogenic process at a tectonic timescale as a steady-state process of Coulomb friction with random fluctuations, and we consider earthquake events to be transient stick–slip events during the process. On the basis of the Langevin equation and its corresponding FPE, we numerically generate stochastic friction processes and derive the theoretical PDF for rupture slips. The results show that both the analytical solution of the FPE and the numerical solutions of the Langevin equation coincide with the truncated exponential (TEX) model proposed by Thingbaijam and Mai (2016). Furthermore, numerical simulation of the Langevin equation suggests a consistent energy–duration scaling law within the additive-noise, Coulomb-damping regime, where the scaling exponent lies in the range of observed moment–duration relationships. The proposed Langevin equation provides a physical basis for understanding the scaling parameter in scaling laws, connecting it to the average dissipative effect, environmental noise effect, and average driving force of a faulting system. These insights into the scaling laws may contribute to future advancements in assessing the potential for earthquake clustering or cascading events in a probabilistic manner.

2. *Stochastic Dynamics for Heterogeneous Friction*

Both frictional slip and rock fracture are the process of degradation of shear strength, with associated dissipation of energy through cracking, plastic deformation or comminution with ongoing slip. With considerable circumstantial evidences, Ohnaka et al. (1997) pointed out that earthquake rupture is a mixed process of frictional slip and fracture of intact rock. Later in Ohnaka (2003), a unified framework for comprehending earthquake, frictional slip, and fracture of rock is established based on laboratory experiments and field observations of earthquakes. The very key role in the unified constitutive law proposed by Ohnaka (2003) is the "characteristic length", which directly associates with the fractal geometrical irregularities and the average size of breakdown zones (also frequently denoted as "asperities" or "barriers") of the faulting surfaces. Breakdown zones refer to strong patches of high rupture resistance on a fault, at which strain energy accumulates during interseismic period. The assumption of heterogeneous strong patches in a fault system sits in the center of the barrier model [e.g.,(Aki, 1979, 1984; Kanamori & Stewart, 1978; Papageorgiou & Aki, 1983)] to explain the dynamics of earthquake as part of the stick–slip behavior in tectonic motion. Based on granite shearing experiments under high confining pressure, it has been suggested that generating a new fracture plane requires identical deformation energy as activating a preexisting fault (Byerlee, 1967; Costamagna et al., 2007), and thus the activation of an earthquake is often put into analogy with the onset of sudden slip of a slider in a spring–slider system.

The simplest representative model treating an earthquake fault system as a many-body system is the spring–block model, with the model of Burridge and Knopoff (1967) being the first of its kind to involve massive blocks. In many studies, an asperity or local strong patch on the sliding surfaces is simplified as an individual strain–energy-storing unit, such as a slider attached by a tensioned spring [e.g., (Burridge & Knopoff, 1967; Gross, 2000)] or a bending bristle [e.g., (de Wit et al., 1995; Haessig & Friedland, 1991; Liang et al., 2012; Saltiel et al., 2017)]. The spring-slider model provides a conceptual framework that connects the Coulomb failure criterion and Griffith's theory of fracture to friction and material failure. The Coulomb failure criterion, which relates shear stress to normal stress, provides a phenomenological description of frictional behavior (Labuz & Zang, 2012). For earthquake rupture, it states that failure occurs when the shear stress reaches a critical strength that depends on material properties and the stress states underground. In the spring–slider model, this critical shear stress corresponds to the point at which the applied force exceeds the frictional resistance, causing the slider to slip. Griffith's theory of fracture, on the other hand, focuses on the energy balance at the rupture front or crack tip (Zang & Stephansson, 2010). According to Griffith's criterion, failure occurs when the available energy (strain or potential energy release minus heat dissipation) exceeds the energy required to create new cracks or surfaces. In the spring-slider model, the rupture front corresponds to the location of the sliding slider, and the energy balance at this front determines whether the slip will keep propagating or cease. If the available energy exceeds the threshold necessary for creating cracks that lead to the activation of adjacent spring–slider units, slip continues, analogous to fracture propagation; otherwise, slip ceases.

Theoretically, we can deterministically predict the evolution of any macroscopic dynamical system with classical mechanics, but for systems with many degrees of freedom, the differential equations become explicitly unsolvable (Eckmann, 1981). With the existence of asymmetry in a spring–slider system, the dynamics of the blocks easily exhibits deterministic chaos, leading to the hypothesis that an earthquake can be treated as a stochastic process (Huang & Turcotte, 1990, 1992; Rundle et al., 2003). In the propagation of rupture within a many-body system such as an earthquake faulting system, the forces at each successive rupture point are practically indeterminate. Aiming for obtaining sufficient number of model-based simulations, we follow Langevin's approach to reduce the number of degrees of freedom by introducing a random force, treating the aggregate dynamics of rupture with a stochastic model for tractability. In Langevin's description for Brownian motion, the motion of Brownian particles in a heat bath is assumed to be memoryless and nondifferentiable (Hanggi & Marchesoni, 2005), and therefore, the total force on a Brownian particle can be subdivided into a deterministic (classical) part and a random (thermodynamic) part. Considering a seismogenic environment where spontaneous failures persistently occur, we categorize the forces governing the dynamics into three terms: external deterministic, internal stochastic, and dissipative. The external driving force is required for the system to reach critical strain and stress conditions; it acts as the tectonic driving force. The internal stochastic force encompasses all internal interactions, including frictional and fracture failures arising from heterogeneous prestressed conditions, as well as collisions between structures. Finally, the presence of a damping term is necessary to dissipate kinetic energy and ensure physical reasonability.

To illustrate the proposed stochastic process for earthquake rupture, we start with a conventional spring-block model, as shown in Fig. 1a. This conceptual model consists of spring–slider pairs lying against the landscape, with arbitrarily scattered obstacles between sliders. In the diagram, obstacles represented by hexagons symbolize a broad sense of energy "sinks" that have to be filled, such as cracking energy, before rupture can progress further. The landscape interacts with sliders through friction, with the varying curvature of the landscape visualizing energy barriers that have to be overcome for rupture to occur. On the other hand, springs serve as units for storing strain energy and mediate interactions between masses. Arrows in the figure further depict forces balanced on a representative block, including

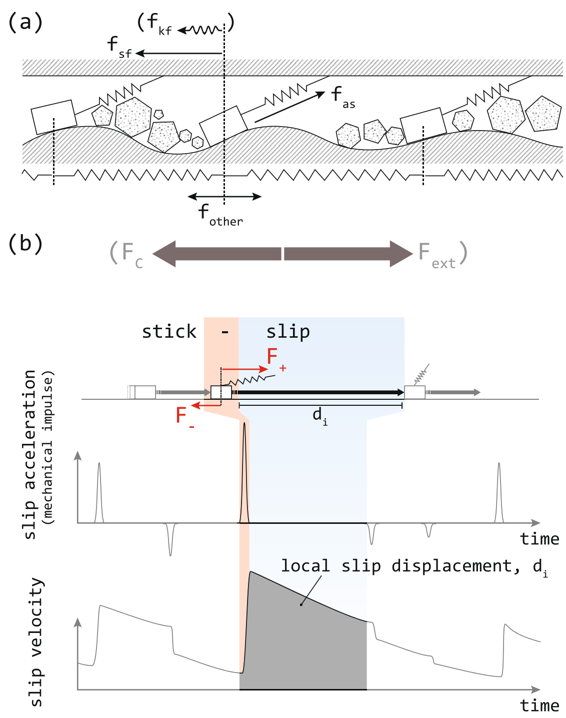

Figure 1
Illustration of our idea of modeling the earthquake source process with the Langevin equation. **a** The illustration of the components of the system. **b** The time-force diagram with one stick–slip step emphasized with color. The resultant force that do positive work is denoted as F_+, and that do negative works is denoted as F_- (with the $+$ and $-$ sign indicating the direction of energy transfer). The mechanical impulse in (**b**) is the sum of F_+ and F_-

kinetic friction (f_{kf}), static friction (f_{sf}), spring force (f_{as}), and interactions between blocks (f_{other}). These forces can be summarized as an equivalent dissipative force (F_C) and a driving force (F_{ext}), as displayed in Fig. 1b, where F_C and F_{ext} act in opposite directions due to their nature.

The net effect of forces balanced on the representative slider at rupture front influences the speed of the rupture and controls its progression; however, it is practically unpredictable, as addressed before. Following Langevin's approach, energy dissipation and momentum transfer in the rupture process are treated separately, with a random force accounting for the unpredictable variation in the momentum of the rupture front. As displayed in Fig. 1b, the stochastic process for earthquake rupture we are going to propose is depicted as a sequence of stick–dissipate-collide events occurring in succession, where each event consists of an abrupt change in slip velocity of a random value and a dissipative phase.

Assuming a simple Coulomb dissipative force, a memoryless random force, and a constant external driving force, the Langevin equation for the stochastic rupture process is formulated as follows:

$$F_k(t) = \frac{\mathrm{d}v(t)}{\mathrm{d}t} = -F_C\frac{v(t)}{|v(t)|} + \Gamma(t) + F_{\mathrm{ext}}. \qquad (1)$$

In this equation, $F_k(t)$ represents the force acting on the system at time t, $\frac{\mathrm{d}v(t)}{\mathrm{d}t}$ is the derivative of the slip velocity with respect to time, F_C is the dissipative force, $v(t)$ is the slip velocity, $\Gamma(t)$ is the memoryless random force, and F_{ext} is the external driving force. Noted that the mass is omitted; the forces in Eq. 1 are all in the sense of "per unit mass".

Equation 1 mathematically construct our conceptual model for earthquake rupture, describing rupture propagation as a step-by-step diffusion–dissipation process. The random force, $\Gamma(t)$, is alternatively called the "diffusional force" since it is the cause that makes the random variable to disperse over time (and the process is thus described to be "diffusive"); its mathematical definition is described in Sect. 3. Without the random force, Eq. 1 describes only the macroscopic behavior of a Coulomb frictional process; that is, a steady rupture just like a block smoothly sliding on table.

3. *Particular Solutions from the Langevin Equation of Coulomb Friction and the Analytic Solution from the Fokker–Planck Equation*

The total force in a Langevin equation is always constituted by two terms: the drift term for deterministic forces and the diffusional term for thermodynamic/random forces. In Eq. 1, the drift term is composed of the damping of Coulomb friction ($-F_C\frac{v(t)}{|v(t)|}$) and the external force (F_{ext}); the diffusional term is the random force ($\Gamma(t)$). The diffusion term $\Gamma(t)$ in Eq. 1 is a time-independent random fluctuating force responsible for chaotic interactions and collisions and is defined by the time derivative of the Wiener process $W(t)$ to enable analytical calculation. By reducing the number of degrees of freedom in the many-body system to only one, the motion of an entity (or a body) in the system can be represented by the motion of the representative Brownian particle. The relation between $\Gamma(t)$ and the standard Wiener process ($W(t)$) is:

$$\Gamma(t) \equiv \sqrt{2D}\mathrm{d}W(t)/\mathrm{d}t, \qquad (2)$$

satisfying (Jazwinski, 1970; Kubo, 1966):

$$\langle\Gamma(t)\Gamma(s)\rangle = 2D\delta(t-s), \qquad (3)$$

where the diffusion coefficient D reflects the average strength of the random fluctuation $\Gamma(t)$. By substituting the random force with the standard Wiener process in Eq. 2, we have the following equivalent stochastic differential equation (SDE) for Eq. 1, with $v(t)$ being the random variable for the (particle) slip velocity:

$$\mathrm{d}v(t) = -F_C\frac{v(t)}{|v(t)|}\mathrm{d}t + F_{\mathrm{ext}}\mathrm{d}t + \sqrt{2D}\mathrm{d}W(t). \qquad (4)$$

In Eq. 4, $\mathrm{d}W(t)$ is also a random variable comprising independent and equally probable Gaussian-distributed steps with standard deviation $\pm\sqrt{\mathrm{d}t}$. Accordingly, a stepwise sample path $v_p(t) = \{V_0, V_1, V_2, \ldots, V_k, \ldots, V_N\}$ can be constructed by subdividing a given time interval $[0, T]$ into N subintervals, $0 = t_0 < t_1 < t_2 < \ldots < t_k < \ldots < t_N = T$, with $V_{k+1} - V_k$ being $(-(F_C V_k/|V_k|) + F_{\mathrm{ext}})(t_{k+1} - t_k) + \sqrt{2D}\mathrm{d}W(t_k)$ (Cyganowski et al., 2001). The Langevin equation is essentially an SDE where the realizations of the random variable (i.e., the particular solutions or sample paths) have little meaning until the statistics are computed. Similar to the deterministic equation of motion (Newton's second law), the Langevin equation has a straightforward physical meaning; however, it cannot predict the exact trajectory of a Brownian particle. Instead, the Langevin equation is usually used to obtain a large number of particular solutions for an ensemble prediction.

The Langevin equation always gives statistically equivalent results as its corresponding FPE, which was demonstrated later (van Kampen, 1981; Lemons & Gythiel, 1997). In contrast to the Langevin equation, the FPE is a partial differential equation that describes the evolution of the probability distribution of a fluctuating macroscopic variable, for example, y.

By solving the FPE, the stochastic process is realized as the evolution of the probability distribution of y, denoted $P(y,t)$. The well-known diffusion equation describing the collective behavior of an assembly of free Brownian particles is a simple example of the FPE (Coffey et al., 1996; van Kampen, 1981). The FPE and the Langevin equation are mathematically equivalent (van Kampen, 1981), but they describe Markovian random walks from two entirely different perspectives. In practice, only a few FPEs can be solved analytically, whereas obtaining the PDF according to particular solutions of the Langevin equation is computationally time-consuming (Zorzano et al., 1999). For the Langevin equation in the form of $\mathrm{d}y(t)/\mathrm{d}t = A(t, y(t)) + \Gamma(t)$, the corresponding FPE is (van Kampen, 1981)

$$\frac{\partial P(y,t)}{\partial t} = -\frac{\partial}{\partial y}\Big(A(t,y(t))P(y,t)\Big) + D\frac{\partial^2}{\partial y^2}P(y,t) \tag{5}$$

By substituting the drift term $A(t, y(t))$ with $-F_C v(t)/|v(t)| + F_{\text{ext}}$, we can obtain the FPE for the stochastic process of Coulomb friction

$$\frac{\partial P(v,t)}{\partial t} = -\frac{\partial}{\partial v}\left(\left(-F_C\frac{v(t)}{|v(t)|} + F_{\text{ext}}\right)P(v,t)\right) + D\frac{\partial^2}{\partial v^2}P(v,t). \tag{6}$$

Assuming steady-state conditions, where the system is far from the initial condition and the process is stationary, meaning that the PDF is invariant with time ($\partial P(v,t)/\partial t = 0$), we have:

$$\left(-F_C\frac{v}{|v|} + F_{\text{ext}}\right)P_{\text{st}}(v) = D\frac{\partial}{\partial v}P_{\text{st}}(v). \tag{7}$$

Hence, the steady-state solution is given by:

$$P_{\text{st}}(v) = P_0 \exp\left(\frac{F_{\text{ext}}v}{D}\right)\exp\left(\frac{-F_C v\frac{v}{|v|}}{D}\right), \tag{8}$$

or simply

$$P_{\text{st}}(v) = \begin{cases} P_0 \exp\left(\frac{F_{\text{ext}}+F_C}{D}v\right), \text{ for } v \le 0 \\ P_0 \exp\left(\frac{F_{\text{ext}}-F_C}{D}v\right), \text{ for } v > 0 \end{cases} \tag{9}$$

4. Results

4.1. The Empirical TEX Model for Inversion-Derived Slips of Large Earthquakes

Equation 9 theoretically shows that the distribution of slip velocities during a steady-state friction process is a double-sided exponential function. As an example, Fig. 2 demonstrates comparisons between the analytically obtained steady-state solutions $P_{\text{st}}(v)$ of the FPE (Eqs. 8 or 9), shown as the red curves, and the ensemble-predicted distributions as histograms, with $D = 10$, $F_C = 1$, and $F_{\text{ext}} = 0.9$. Each histogram subplot comprises values sampled from 10^4 sample paths of $v(t)$ at $t = 713$, 1571, 2428, 3285, 4143, and 5000, with each sample path being obtained by numerically solving the Langevin equation (Eqs. 1 or 4). The red curves in the figure are the theoretical probability distributions of v at $t \to \infty$; as a matter of course, the histograms of the ensemble-predicted values at larger t approximate the red curves better than those at smaller t.

For real large earthquakes ($M_w \ge 5$), Thingbaijam and Mai demonstrated that the TEX distribution best characterizes the empirical distribution of rupture slips in either an individual or an average sense, as demonstrated in Fig. 3. The authors examined the goodness of fit rigorously over the TEX distribution in addition to other well-known distributions, including the exponential (EXP), Weibull, Gamma, and lognormal distributions, by analyzing 190 source models of events worldwide. They concluded that the TEX distribution generally exhibits the best fit to the slips along fault planes, especially at larger slip values. In their study, the fitting function was expressed in the form of the complementary cumulative distribution function (CCDF) to avoid arbitrarily choosing the data bin size and to better distinguish the fitting results at large slips. In addition, the CCDF for a non-truncated EXP

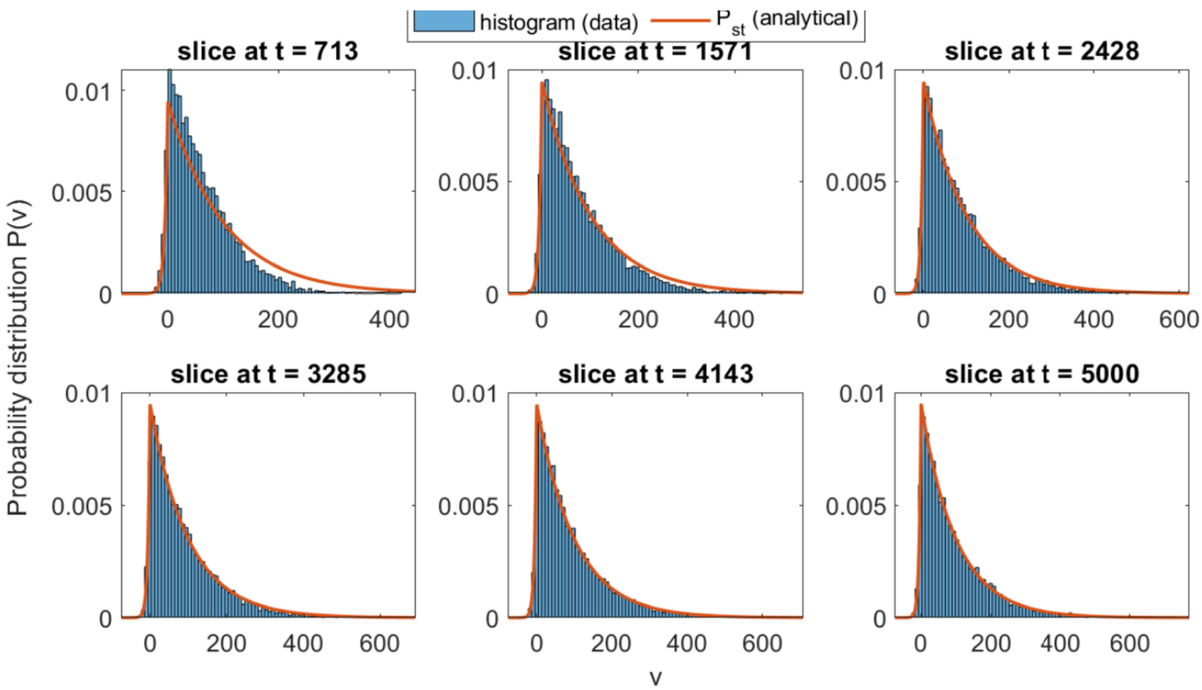

Figure 2
The probability distribution of slip velocity calculated from an ensemble of samples sampled from total 10^4 realizations at different time (the histogram), and the steady-state solution $P_{st}(v)$ (see Eqs. 8 and 9) (the red curve), in which $D = 10$, $F_C = 1$, $F_{ext} = 0.9$

distribution function $f_{EXP}(v) = (1/v_c)\exp(-v/v_c)$ is also an EXP distribution:

$$1 - F_{EXP}(v) = \exp\left(-\frac{v}{v_c}\right), \tag{10}$$

where $F_{EXP}(v) = 1 - \exp(-v/v_c)$ is the cumulative distribution function (CDF) of $f_{EXP}(v)$. For the TEX distribution $f_{TEX}(v) \equiv f_{EXP}(v)/F_{EXP}(v_{max})$, its CCDF form is

$$1 - F_{TEX}(v) = \frac{\exp(-v/v_c) - \exp(-v_{max}/v_c)}{1 - \exp(-v_{max}/v_c)}, \tag{11}$$

where $F_{TEX}(v)$ is the CDF of $f_{TEX}(v)$. The TEX distribution function is a conditional distribution obtained by restricting the domain of the original function. When calculating the distribution of either a simulated or an empirically observed physical quantity, the largest value in the dataset must be finite. Thus, empirically calculated statistics can more often fit the TEX distribution better than the original form can.

To demonstrates how local slips ($(t_{k+1} - t_k)V_k$ or $v_p(t)dt$) in an individual realization of the Langevin friction process fit the TEX and EXP functions, we generate three sample paths of different durations with the parameters $D = 5$, $F_C = 1$, and $F_{ext} = 0.9$. Relatively large values of D and F_{ext} (relative to F_C) are chosen because they generally produce larger slips and might better meet the physical conditions for large earthquakes. Following the method of Thingbaijam and Mai, we calculate the CCDF of slip velocities for an individual realization or set of realizations and fit their CCDF with the CCDFs of the EXP (Eq. 10) and TEX (Eq. 11) distribution functions. The fitting results are demonstrated in Fig. 4. The scale parameters (v_c) are estimated by nonlinear least-squares fitting of the TEX or EXP model to the empirical CDF. In Fig. 4a–c, the empirical CDF is the slip velocity distribution with uniform temporal sampling from one realization of the stochastic process, and the durations are 100, 1000, and 10,000 simulation times (s.t.), respectively. In Fig. 4c–f, the empirical CDF is calculated in the same way but from 1000 realizations for each

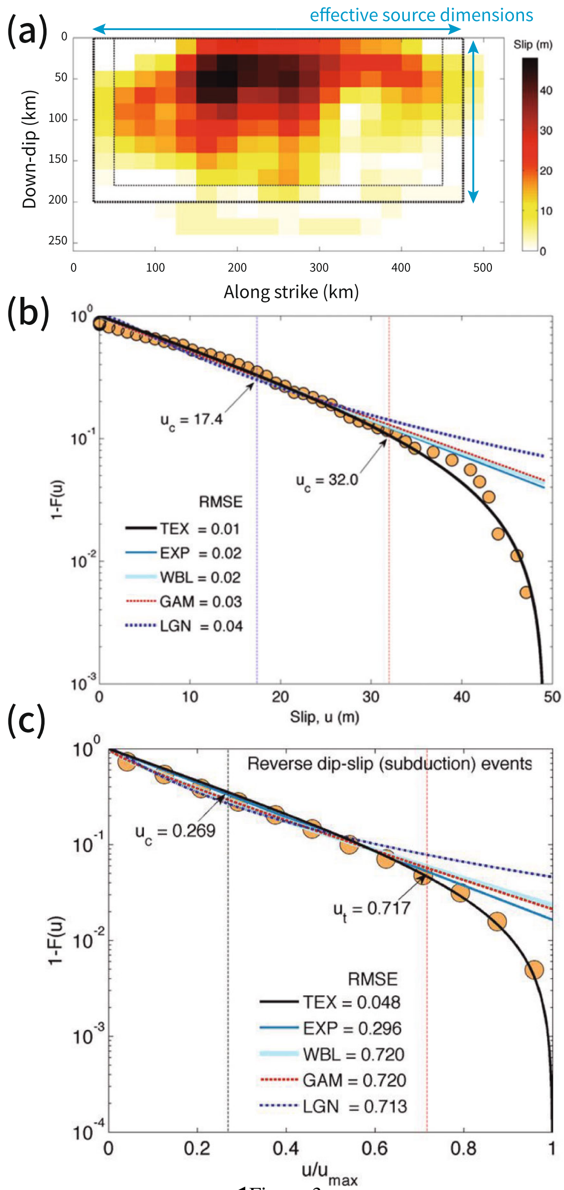

◀Figure 3

The empirical TEX law for earthquake rupture slips proposed by Thingbaijam and Mai (2016). **a** [modified from Fig. 1a in Thingbaijam and Mai (2016)] The slip distribution from the finite source inversion for the 2011 Tohoku earthquake. **b** [Fig. 1b in Thingbaijam and Mai (2016)] The CCDF of the slip distribution of (**a**). In this subplot, orange circles denotes the empirical CCDF computed from the source model that is trimmed to the effective source dimensions; colored-solid or -dashed lines denotes the best fitting models of various distribution functions. **c** [the upper-left panel in the Fig. 4 of Thingbaijam and Mai (2016)] The averaged CCDF of the slip distributions of subduction zone earthquakes worldwide. For the EXP and TEX distribution function, see Eqs. 10 and 11 in this study; for the Weibull (WBL), Gamma (GAM) and lognormal (LGN) distributions, please refer to the Table 1 in the study of Thingbaijam and Mai (2016)

duration to ensure that the result is robust. Note that we take the modulus of the signed velocities before calculating the CDF; that is, the absolute values of the negative velocities are added to the population of positive values. The results show that for sample paths of either short or long duration, the distribution exhibits a TEX shape and generally fits a TEX distribution better than an EXP distribution (i.e., the TEX fitting exhibits a lower R-squared (R^2) value or mean squared error (MSE)). Eq. 9 demonstrates the theoretical probability distribution (P_{st}) for the slip velocity of a steady-state Coulomb friction process. Using integration by parts, we can obtain the expectation $\langle v\rangle$ by treating positive and negative velocities separately:

$$\langle v\rangle = \int_{-\infty}^{\infty} vP_{st}(v)\mathrm{d}v = -\frac{2DF_{ext}}{F_{ext}^2 - F_C^2}, \tag{12}$$

where

$$\langle v^-\rangle = \int_{-\infty}^{0} vP_{st}(v)\mathrm{d}v = -\frac{D}{2F_C}\frac{F_C - F_{ext}}{F_{ext} + F_C} \tag{13}$$

and

$$\langle v^+\rangle = \int_{0}^{\infty} vP_{st}(v)\mathrm{d}v = -\frac{D}{2F_C}\frac{F_C + F_{ext}}{F_{ext} - F_C}, \tag{14}$$

with F_{ext} assumed to be positive. As demonstrated by Eq. 12, F_{ext} critically contributes to the expected velocity ($\langle v\rangle$), especially when $F_{ext} \rightarrow F_C$. For example, in the case of $F_{ext} = 0.9F_C$, $|\langle v\rangle|$ is nearly 47 times greater than that in the case of $F_{ext} = 0.1F_C$ given the same D. Furthermore, in the case of $F_{ext} = 0.9F_C$ with $F_{ext} > 0$, positive velocities are overwhelmingly dominant in the population, as we have $|\langle v^+\rangle|/|\langle v^-\rangle| = 361$. In this case, owing to the decay exponent for $v < 0$ (i.e., $1.9F_C/D$) being much larger than that for $v > 0$ (i.e., $0.1F_C/D$), according to Eq. 9, the probability density decays very quickly, as exemplified in Fig. 2. The EXP model and its truncated form, the TEX distribution, were established based on large events, while the physical condition reflected by large F_{ext}/F_C is particularly favorable for generating large events in our simulation. Thus, the relationships between the scale parameter (u_c in Fig. 3 or v_c in Fig. 4) and the physical parameters in the Langevin equation (F_{ext}, F_C and D) can be derived, as the FPE solution generally approximates a

Table 1

The nonlinear fit to energy dissipated ($E_{\mathrm{diss}} = F_C d$) and durations T of events with $\ln T = c_1 + c_2 \ln E_{\mathrm{diss}}$. Events are defined by threshold $thr = 0$ from particular solutions generated with different diffusion coefficient (D), Coulomb friction parameter (F_C), and external force (F_{ext}) denoted in each row

D	F_C	F_{ext}	$\langle v \rangle$	c_1	c_2
0.1	0.1	0.01	0.20	2.39	0.65
0.1	0.1	0.05	1.33	2.58	0.57
0.1	0.1	0.09	9.47	2.18	0.72
0.1	10	1	0.00	−2.04	0.41
0.1	10	5	0.01	−1.07	0.57
0.1	10	9	0.09	−0.67	0.65
0.1	1	0.1	0.02	0.73	0.62
0.1	1	0.5	0.13	0.83	0.64
0.1	1	0.9	0.95	0.91	0.66
1	0.1	0.01	2.02	1.70	0.65
1	0.1	0.05	13.33	1.63	0.66
1	0.1	0.09	94.74	2.16	0.61
1	10	1	0.02	−1.51	0.61
1	10	5	0.13	−1.44	0.64
1	10	9	0.95	−1.34	0.64
1	1	0.1	0.20	0.08	0.66
1	1	0.5	1.33	0.10	0.66
1	1	0.9	9.47	0.13	0.65
10	0.1	0.01	20.20	0.67	0.69
10	0.1	0.05	133.33	0.59	0.69
10	0.1	0.09	947.37	−0.17	0.75
10	10	1	0.20	−2.11	0.61
10	10	5	1.33	−2.12	0.63
10	10	9	9.47	−2.13	0.65
10	1	0.1	2.02	−0.56	0.64
10	1	0.5	13.33	−1.31	0.75
10	1	0.9	94.74	−0.84	0.68

single-sided exponential function for large F_{ext}/F_C according to Eq. 9. The single-sided exponential function (e.g., $P_0 \exp\left(\frac{F_{\mathrm{ext}}-F_C}{D} v\right)$ for $F_{\mathrm{ext}} > 0$) can be rewritten as the EXP model $P_0 \exp(-v/v_c)$. Hence, the relationship $v_c \equiv -\frac{D}{F_{\mathrm{ext}}-F_C}$ is derived, providing a physical interpretation for the empirical TEX model for earthquake rupture slips.

4.2. The Energy–Duration Scaling of the Simulated Events

The total energy released in an earthquake is the work done by the mean absolute shear stress ($\bar{\sigma}$) over the average slip distance ($\bar{d}$); it has the following relationship with the seismic moment (Kanamori & Anderson, 1975):

$$E = \bar{\sigma} S \bar{d} = \frac{\bar{\sigma}}{\mu} M_0. \tag{15}$$

Since practically quantifying the absolute shear stress is impossible, the total energy released in an earthquake event can be obtained only indirectly via a certain empirical relation; mostly, it is estimated as a portion of the seismic moment (M_0). Seismic moment has the dimensions of torque, being an equivalent representation of earthquake sources as a double-couple; it is defined as $M_0 = \mu S \bar{d}$ where μ is the rigidity, S the area of the fault, and $\bar{d}$ the mean slip displacement (Aki, 1972). Following the idea that an earthquake is decomposable, the equivalent double-couple of an event is thus a composition of a collection of smaller double-couples, with each resulting in a stick–slip event. Now go back to Eq. 1, in our spatially 0-D model (a 1-D Langevin equation for the

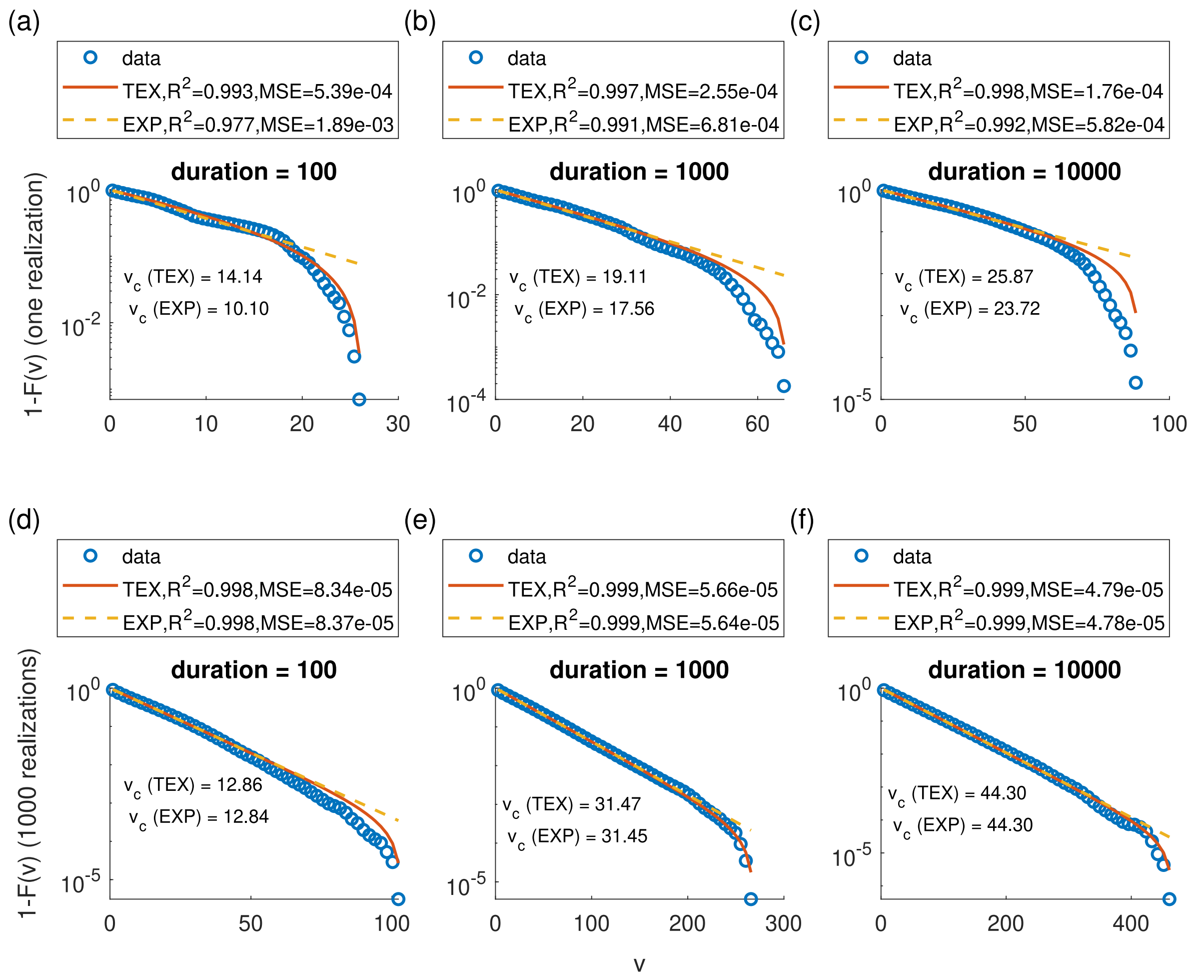

Figure 4
The CCDF of synthetic slip velocities of different durations ($T = 10$, 100, and 1000), and their best fitting TEX and EXP model (red solid and orange dashed curve, respectively). The slip velocities are sampled evenly spaced in time from the particular solutions of Eq. 4, where $D = 5,\ F_C = 1,\ F_{\text{ext}} = 0.9$. In **a**, **b**, and **c**, velocities for each distribution are collected from a single realization; in **d**, **e**, and **f**, velocities for each distribution are collected from 1000 realization

scalar slip velocity) the concept of “area” does not exist, and the total amount of energy released in stick–slip eventually equals the energy dissipated in the friction process. Thus, we let the term $-F_C v/|v|$ in Eq. 1 to play the role of the term $\bar{\sigma}S$ in Eq. 15 that we can have discussions on the issue of energy–duration relation. The energy dissipated (E_{diss}) in a realization ($v_p(t)$) of the stochastic process can be calculated simply by

$$E_{\text{diss}} = \int_{x=0}^{d} F_C \mathrm{d}x = \int_{t=0}^{T} F_C v_p(t) \mathrm{d}t. \tag{16}$$

Then, assuming a constant Coulomb friction, the total amount of energy dissipated by the representative Brownian particle is $E_{\text{diss}} = F_C d$, where d is the accumulated slip during the process, as follows:

$$E_{\text{diss}} \propto d = \int_{t=0}^{T} v_p(t) \mathrm{d}t \tag{17}$$

For a physically reasonable system, the absolute value of the driving force (F_{ext}) should lie within

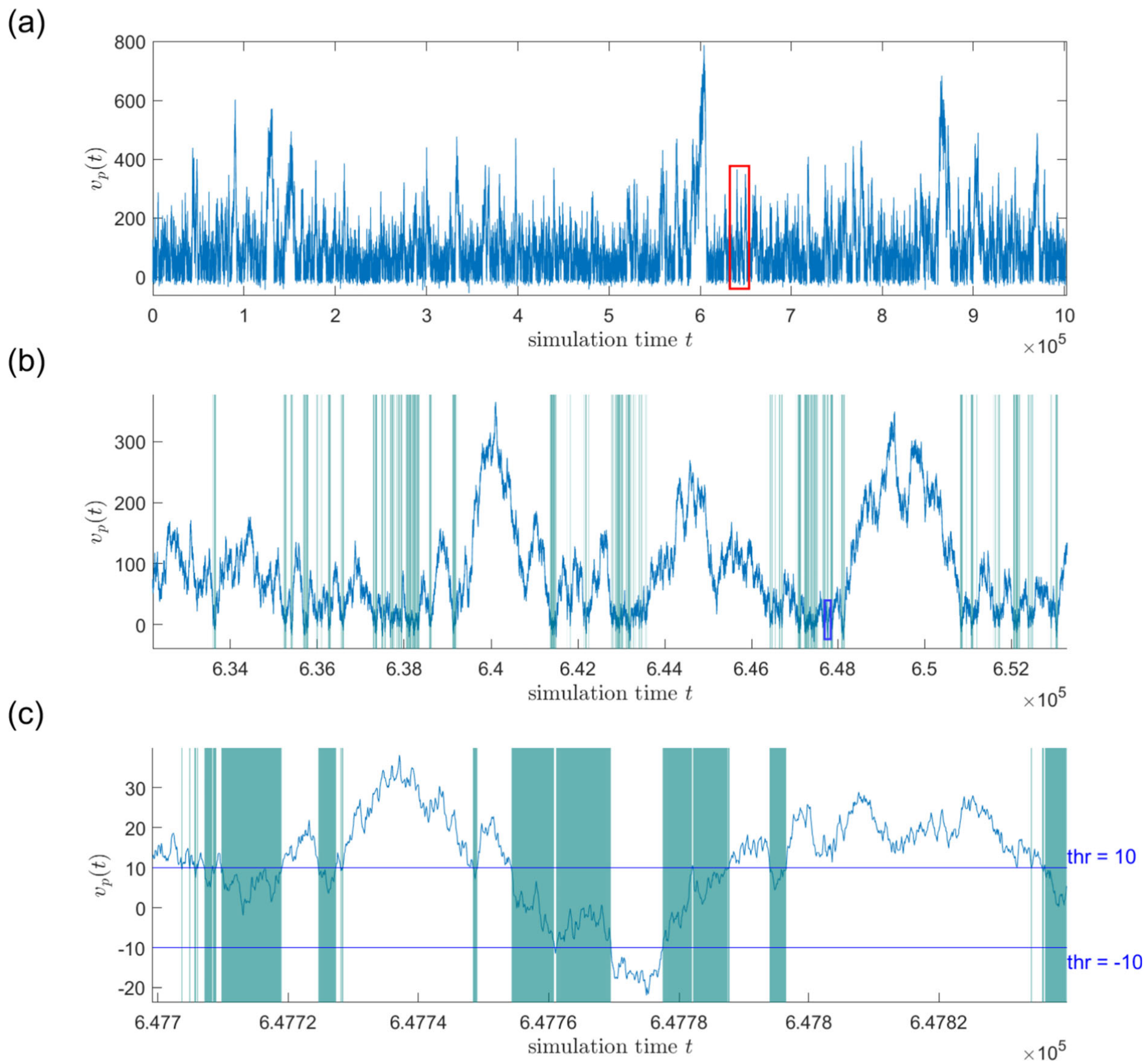

Figure 5
The demonstration of how a sample path obtained from numerically solving the Langevin equation is subdivided into segments (namely, simulated events) in this study, with an exemplary threshold of detection $v_{\mathrm{thr}} = 10$. **a** The entire sample path of $T \approx 10^6$ simulation time, with $D = 10,\ F_C = 1,\ F_{\mathrm{ext}} = 0.9$. **b** Zoom up of (**a**) (red region in (**a**)). **c** Zoom up of (**b**) (blue rectangle in (**b**)). In subplots (**b**) and (**c**), the shaded area marks the intervals in which $|v_p(t)| \le v_{\mathrm{thr}}$ is satisfied, being the divisions between events

$\pm F_C$; otherwise, the diffusion process eventually diverges. When simulating the friction process of a tectonic plate, $F_{\mathrm{ext}} = 0$ represents the condition under no tectonic stress, and local slips equally favor any direction; in contrast, if $F_{\mathrm{ext}} = \pm F_C$, the process is close to diverging (i.e., $v \to \pm\infty$ as $t \to \infty$). Figure 5a demonstrates an example of a sample path, which is a realization of the slip velocity history as a particular solution of the Langevin equation (Eq. 4) with $F_C = 1$, $F_{\mathrm{ext}} = 0.9$, and $D = 10$. By regarding an earthquake event (or a series of events) as a realization of the stochastic process governed by the Langevin equation, we define a simulated event as a segment of the particular solution divided by a certain threshold. That is, a simulated event starts when the slip velocity (v) of the representative Brownian particle exceeds a certain threshold and ends when v falls below that same threshold. The subdivision of an event is illustrated in Fig. 5b, c. The shaded areas in (b) and (c) indicate the intervals in which the sampled velocities all fall below the threshold $v_{\text{thr}} = 10$ and are thus regarded as "undetectable" activities; in contrast, the intervals with an unshaded background (where $v > v_{\text{thr}}$) are hence regarded as the durations of the simulated events. To replicate the scenario of a tectonic process in which local slips are expected to favor a certain direction, we choose F_{ext} values of $+0.1F_C$, $+0.5F_C$, and $+0.9F_C$ against the diffusion coefficient $D = \{0.1, 1, 10\}$, and friction parameter $F_C = \{0.1, 1, 10\}$. We then generate a set of particular solutions of duration $\approx 10^6$ s.t. with a step size of $\mathrm{d}t = 10^{-3}$ (s.t.); that is, we establish a set of sample paths, with each path having $\sim 10^9$ steps. The numerical solutions are calculated according to Eq. 4 in an Eulerian scheme following the instruction manual of Cyganowski et al. (2001). By defining the lengths of the time series divided by the threshold $v_{\text{thr}} = 0$ as the durations (T) of the simulated events, we calculate the energy dissipated (E_{diss}) in each event according to Eq. 16 to obtain the energy–duration relationship by fitting the data with

$$\ln T = c_1 + c_2 \ln E_{\text{diss}}. \tag{18}$$

The results are demonstrated in Table 1 and plotted in Fig. 6, showing that there is no obvious change in the exponent (c_2) of the scaling law (Eq. 18) over a wide range of physical conditions (parameter settings). The best-fitting c_2 is most commonly approximately $2/3$; however, in a few cases, such as the sets of $\{D = 0.1, F_C = 10, F_{\text{ext}} = 1\}$ and $\{D = 0.1, F_C = 10, F_{\text{ext}} = 5\}$, significant deviations of the best-fitting c_2 from $2/3$ are observed. These deviations appear to be especially prominent when the population of a set is dominated by events with durations very close to the temporal resolution ($\mathrm{d}t = 10^{-3}$) of the numerical simulation, that is, under the physical conditions that are favorable for generating very small events (e.g., high F_C and low D and F_{ext}). As observed in every $E_{\text{diss}} - T$ plot of Fig. 6 at approximately $T = 10^{-2}$ and below, the energies of the shortest events exhibit exceptionally broad scatter, largely because of the limitation imposed by the temporal resolution. In other words, the nonlinear fits can deviate considerably as a result of these widely scattered data when they compose the bulk of the population. Overall, it is clear that for all sets of physical conditions, the data points align well with the contour lines of $\ln T = c_1 + (2/3)\ln E_{\text{diss}}$, suggesting an invariant $E_{\text{diss}} - T$ scaling law.

4.3. Spectral Analysis of Velocity Fluctuations

The nearly invariant energy–duration scaling across wide changes in D, F_C, and F_{ext} implies that event time histories are governed by a single rate-limiting timescale rather than a broad cascade; this motivates a closer look at their frequency content. The theoretical foundation for our spectral analysis of the Coulomb-friction process is based on the well-established framework that links exponential auto-correlations to Lorentzian power spectra via the Wiener–Khinchin theorem (Gardiner, 2004; Pavliotis, 2014). In our Coulomb-friction model, a dominant slow relaxation mode yields an approximately exponential velocity autocovariance. By applying the Wiener–Khinchin theorem, we obtain the fitted amplitude spectrum

$$S_v^{(f)}(f) = \frac{S_v^{(f)}(0)}{\sqrt{1 + (f/f_c)^2}}, \tag{19}$$

where the corner frequency f_c is the slowest nonzero relaxation rate. This rate follows from the spectrum of the system's Fokker–Planck operator, which we obtain using methods analogous to those for a Schrödinger equation (see Appendix A.2). For the V-shaped potential associated with Coulomb friction, $U(v) = F_C|v| - F_{\text{ext}}v$, the slowest rate is determined by the lower edge of the operator's continuous spectrum. As shown in Appendix A.1, the corner frequency is

$$f_c = \frac{g(\rho)\left(F_C^2 - F_{\text{ext}}^2\right)}{2\pi D}, \qquad g(\rho) = \frac{1-\rho}{4(1+\rho)}, \tag{20}$$

with the load ratio defined as $\rho = |F_{\text{ext}}|/F_C$. In dimensionless form,

$$\tilde{f}_{c,edge}(\rho) = \frac{(1-\rho)^2}{8\pi}. \tag{21}$$

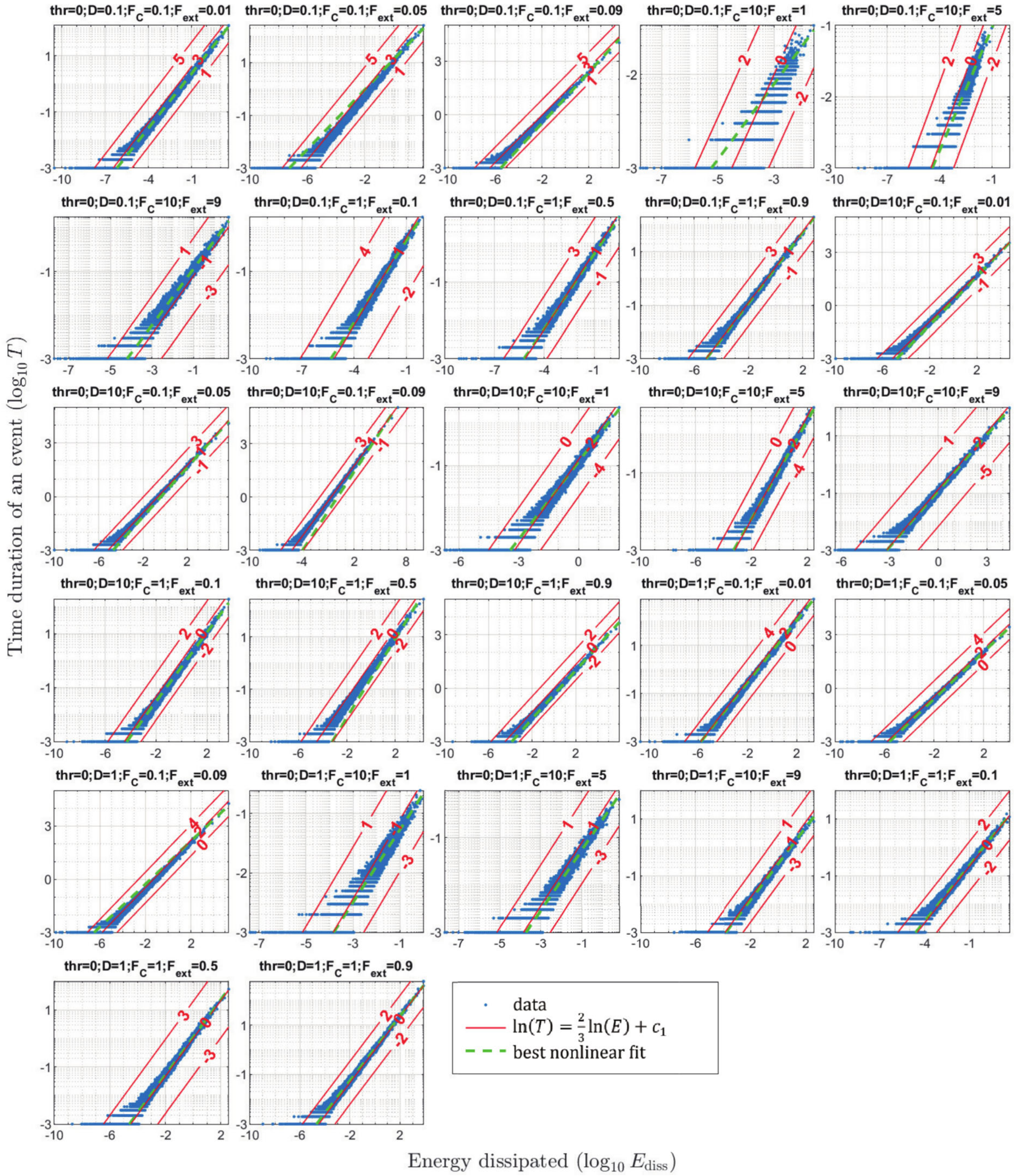

Figure 6

The energies dissipated in and the durations of the simulated events generated by the Langevin equation of Coulomb friction (Eqs. 1 and 4). The threshold defining an detectable event is $v_{\text{thr}} = 0$. The particular solutions are generated with $D = \{0.1, 1, 10\}$, $F_C = \{0.1, 1, 10\}$ and $F_{\text{ext}} = \{0.1F_C, 0.5F_C, 0.9F_C\}$. In each panel, the green dashed line is the best nonlinear fit to the data, with the fitting parameters of each fit (intercept c_1 and slope c_2 in log space) listed in Table 1; the red solid lines are the contour of $c_1 = \ln T - (2/3)\ln E$

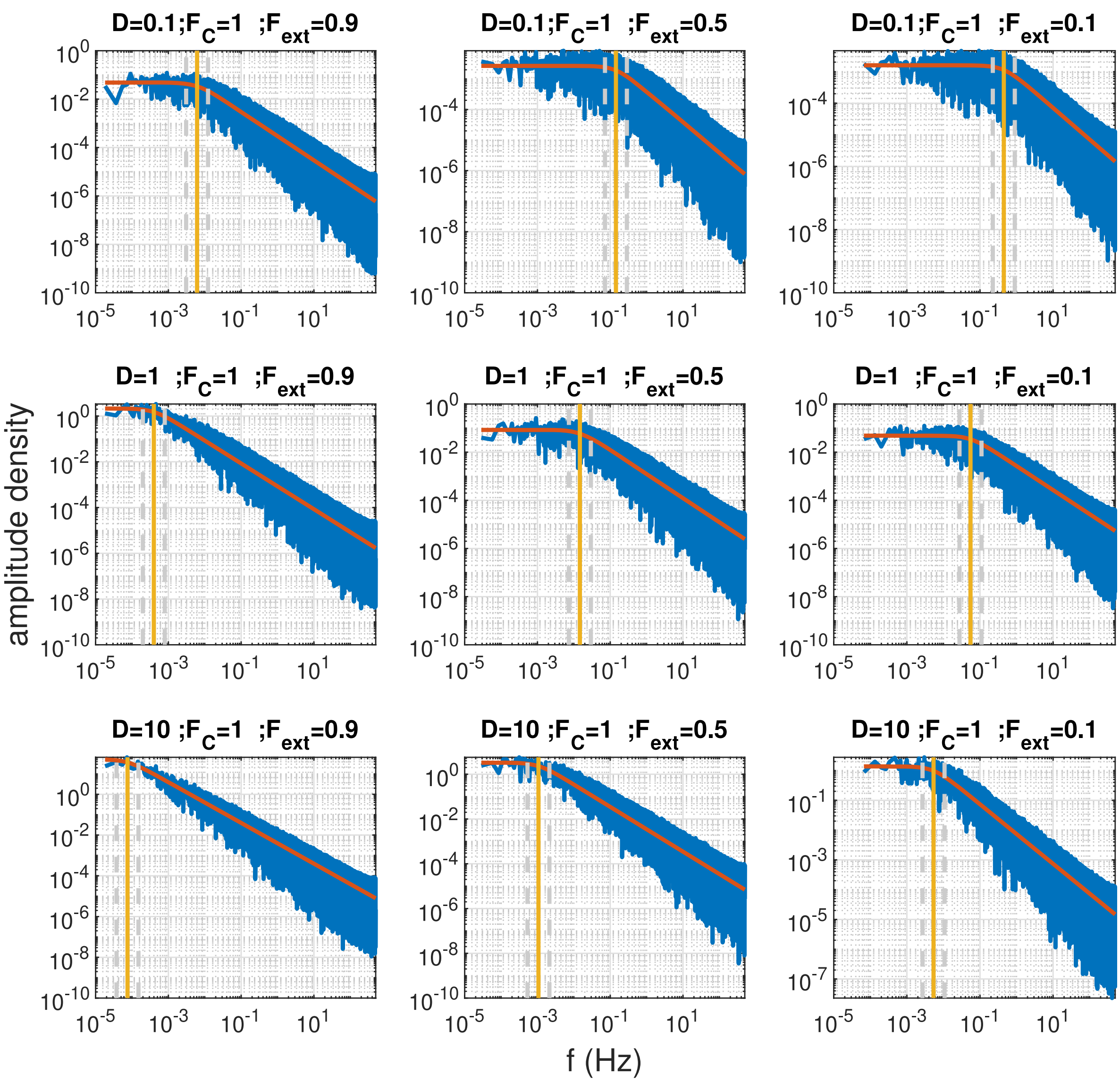

Figure 7

Fourier amplitude spectra of individual events. Each spectrum displays amplitude density as a function of frequency f; corner frequencies f_c are estimated by fitting the Lorentzian model (red curve) to the observed spectral rollover using nonlinear least squares. The simulation events correspond to parameter combinations with $F_C = 1.0$ and three diffusion strengths $D \in \{0.1, 1.0, 10.0\}$ crossed with three external force ratios $\rho = F_{\text{ext}}/F_C \in \{0.1, 0.5, 0.9\}$. In each subplot the yellow solid vertical line marks the estimated f_c; the two gray dashed vertical lines show the range $2^{\pm 1} f_c$ as a visual guide to the uncertainty in the corner-frequency estimate. These f_c estimates are used for the comparisons in Figs. 8 and 9

Fig. 7 shows that the velocity spectra from our Coulomb-friction simulations exhibit single-corner behavior, where each event spectrum fits the Lorentzian amplitude model of Eq. 19 despite the nonlinear nature of the dry-friction process. The corner frequencies f_c estimated from these single-pole fits are compared with theoretical predictions in Fig. 8, showing a systematical agreement with the scaling in Eq. 20. Furthermore, Fig. 9 demonstrates that the load ratio ρ controls the spectral corner. This

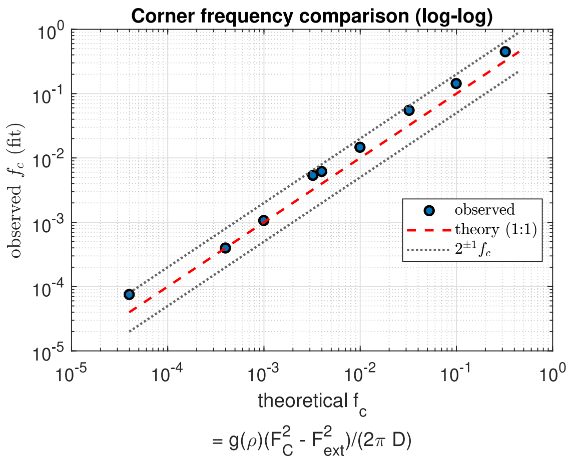

Figure 8
Observed corner frequencies f_c estimated from Fig. 7 compared with the theoretical scaling from the Coulomb-friction Langevin model, plotted on log-log axes. The red dashed line shows the theoretical prediction; gray dotted lines indicate $2^{\pm 1} f_c$ bounds used to assess agreement between observations and theory

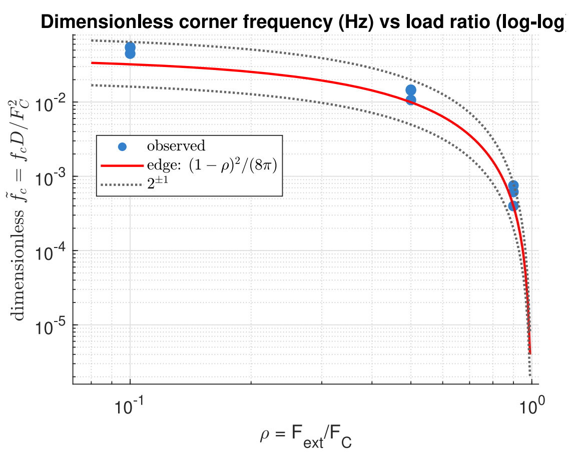

Figure 9
Predicted dependence of the normalized (dimensionless) corner frequency $\tilde{f}_c$ on the load ratio ρ from the Coulomb-friction Langevin model. The red solid line shows the theoretical edge prediction (Eq. 21), with gray dotted lines marking $2^{\pm 1}$ bounds for reference. Blue filled circles show observed values from the simulations. This reference curve summarizes how loading controls the spectral corner and helps interpret the observations compared in Fig. 8

dimensionless corner frequency $\tilde{f}_c$ follows the theoretical edge prediction of Eq. 21, indicating that the corner frequency is governed by proximity to force balance, with $f_c \to 0$ as $\rho \to 1$.

5. *Discussion*

5.1. *Physical Interpretation of the Spectral Corner*

The spectral analysis of velocity fluctuations presented in Sect. 4.3 gives key physical insight into the stochastic Coulomb-friction model. The single-corner shape of the velocity spectra (Fig. 7) suggests the system memory is governed by a characteristic timescale, analogous in its correlations to an Ornstein–Uhlenbeck process even though the underlying drift remains nonlinear which originates from Coulomb friction. This characteristic time, quantified by the corner frequency f_c, reflects a competition between frictional dissipation, which erases memory, and external driving, which sustains motion. The universal scaling of the dimensionless corner frequency with the load ratio, $\tilde{f}_c(\rho)$, confirms that this relaxation time is physically controlled by the balance between internal dissipation and external driving. As the system nears the critical state of force balance ($\rho \to 1$), the relaxation time lengthens and f_c approaches zero, showing that the process maintains its velocity fluctuations for longer periods. This force-balance threshold links the model parameters to the observed temporal behavior.

The functional form of Eq. 19 resembles that used to describe moment-rate spectra of slow earthquakes and tectonic tremor [e.g.,(Ide & Yabe, 2019)]. This correspondence arises because both phenomena can be modeled as processes with exponentially decaying autocorrelation functions, which via the Wiener–Khinchin theorem produce Lorentzian spectra. However, the physical origin of the corner frequency differs between models. In our model it denotes the relaxation rate of velocity fluctuations controlled by force balance, while in Ide's formulation it is tied to relaxation of the slow-slip area.

5.2. *The Energy–Duration Scaling*

Basing on the Langevin equation, we study the energy–duration relationships of a set of simulated events under different physical conditions, with each subset having different parameter settings of F_C, F_{ext}, and D. In each subset, the energies dissipated (E_{diss}) in the 0-D Langevin friction process scale with the event durations (T) with a nearly constant exponent of $2/3$. The parameter settings vary widely, and thus, the average slip velocity expected for the events in each subset may span several orders of magnitude; however, the proportionality between E_{diss} and T in the log space barely changes, suggesting a consistent scaling relationship between the energies dissipated and the event durations within the additive-noise, Coulomb-damping regime. Likewise, seismological observations tend to suggest a universal scaling relationship between the seismic moment and the event duration. Many studies have theoretically derived or empirically observed a scaling relationship of $T \propto M_0^{1/3}$ for regular ("fast") earthquakes (Furumoto & Nakanishi, 1983; Houston, 2001; Kanamori & Anderson, 1975; Michel et al., 2019; Tanioka & Ruff, 1997). In contrast, for slow earthquakes, a scaling law of $T \propto M_0$ has been observed worldwide for non-volcanic tremors, low- or very-low-frequency earthquakes, and slow slip events (Aguiar et al., 2009; Gao et al., 2012; Ide et al., 2007). Due to the difference in the scaling exponent between these two scaling laws, the underlying dynamics were thought to be fundamentally different for fast and slow earthquakes (Ide, 2008; Ide et al., 2007). In a subsequent study conducted by Gomberg et al. (2016), a transition in the scaling exponent of the power law was observed in both fast and slow slip populations. Relying solely on the dislocation theory (Kanamori & Anderson, 1975; Scholz, 1982), the authors concluded that the transition from $T \propto M_0^{1/3}$ to $T \propto M_0$ could originate from the geometric change in rupture growth from two dimensions to a single dimension: for bounded (one-dimensional) ruptures, their results suggest $T \propto M_0$ with the W-model assumption and $T \propto M_0^{1/2}$ with the L-model assumption but suggest $T \propto M_0^{1/3}$ with either the W-model or the L-model assumption for unbounded (two-dimensional) ruptures. A more recent study (Michel et al., 2019) further indicated that the $T \propto M_0$ scaling law for slow earthquakes could arise from the assembling of slow slip events under different physical conditions and reported that the scaling should be $T \propto M_0^{1/3}$ for a subset of slow slip events under the same physical conditions, implying that the underlying dynamics for slow and fast ruptures could be similar. Other studies have proposed or reported that the exponent n of the power law $T \propto M_0^n$ should lie between $1/3$ and 1 (Frank et al., 2018; Ide, 2008; Ide et al., 2008; Thøgersen et al., 2019), and the discrepancies in the moment–duration scaling law were attributed to the lower dimensionality of the model (Thøgersen et al., 2019), different sensory thresholds (Ide, 2008), an artificially limited frequency range (Ide et al., 2008), or the criteria for defining an event (Frank et al., 2018).

Whether there exists a universal moment–duration scaling for either fast or slow earthquakes is still under debate. The nearly invariant energy–duration scaling obtained in this study within our modeling framework could provide insights into the moment–duration scaling law for real earthquakes; however, many questions remain unanswered. First, the seismic moment is simply an attainable substitute for the energy released during the seismogenic process. In other words, for real earthquakes, the seismically or aseismically released energy can only be very roughly obtained through its relation to the seismic moment; for our model, to produce the physical "moment", the relationships between the material rigidity and both the friction parameter and the diffusion coefficient in the governing equation must be established first. Second, we must develop a more complete understanding of the factors that may result in the transition of the scaling exponent but are otherwise unrelated to the underlying physical mechanism, for example, the dimensionality of the system or the criteria for defining an event. In this study, the proposed Langevin equation of friction is for a one-dimensional velocity space. Thus, the exponent in the scaling relationship may experience a transition if the equation is generalized for a space of two or more dimensions. In addition, the threshold for dividing the sample paths into simulated events is zero, which represents an unrealistic noise- and attenuation-free environment in which any activities with a slip velocity greater than zero are detectable. As the threshold changes, the exponent of the power law may change (displayed in the example of Fig. 10). Another issue is that the obtained energy–duration scaling, $T \propto E_{\mathrm{diss}}^{2/3}$, is based solely on numerical simulations. Although this relationship is concluded according to simulations that cover several orders of magnitude of the friction and diffusion coefficient,

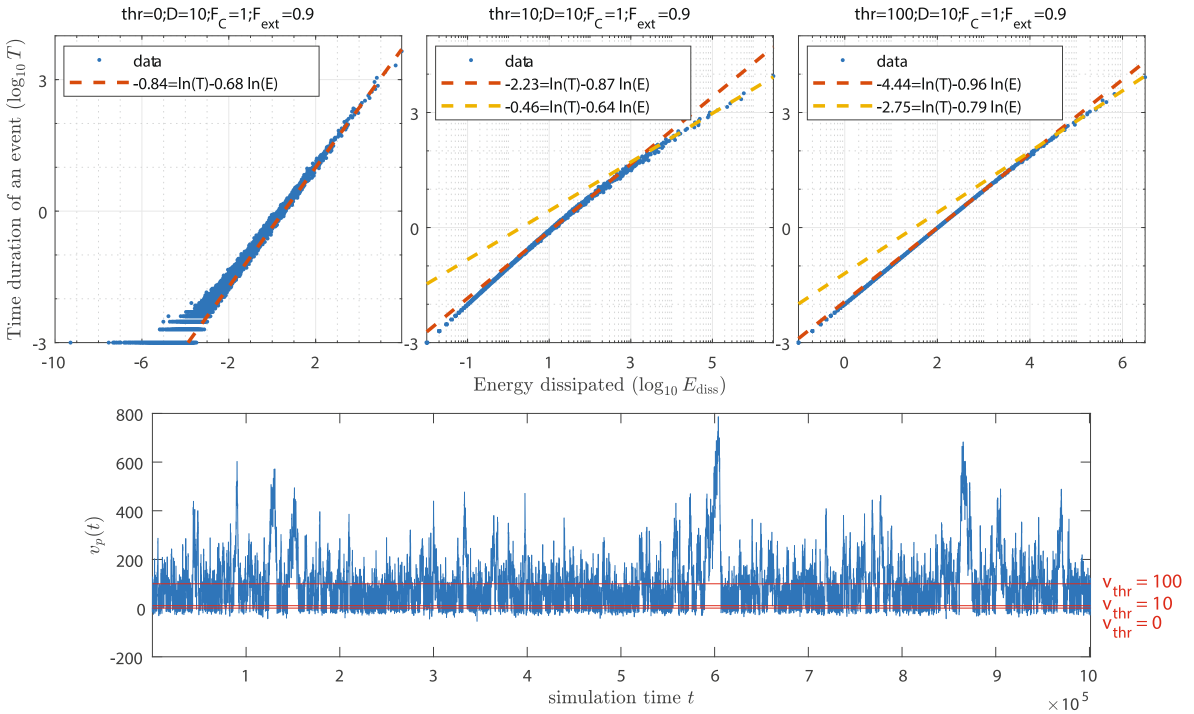

Figure 10
The total energies dissipated v.s. the durations of simulated events defined by different thresholds (namely, $v_{\mathrm{thr}} = 0,\ 10,\ 100$); the particular solution is generated with $D = 10,\ F_C = 1,\ F_{\mathrm{ext}} = 0.9$

much more cases remain untested. We may further narrow down the range of parameters according to the physical condition under which real-world earthquakes possibly occur and conduct a more complete analysis, if the link between the parameters in the Langevin equation to the real-world measurables is established. However, inductive reasoning by itself can never constitute a proof, no matter how many physical conditions have been tested; thus, analytical descriptions are required to explore this issue in greater depth.

5.3. Connection to the Empirical TEX Model for Inversion-Derived Slips of Large Earthquakes

For large F_{ext}/F_C ratios, our theoretical analysis shows that the ensemble-averaged slip distribution should approximate an EXP distribution, and the time-averaged distribution of slips in sample paths of a certain finite length generally fits the TEX function better than it fits the EXP function. These results provide an alternative physical basis for the empirical TEX distribution of rupture slips obtained from finite-source inversions of large earthquakes and suggest that the scale parameter (denoted v_c or u_c) in the TEX or EXP model can be linked to the underlying physical parameters (i.e. D, F_C, and F_{ext}) for generating the earthquake. The ensemble-averaged distribution is the distribution of data sampled at the same time point from a number of realizations of the random variable, while the time-averaged distribution is the distribution of data sampled from a single realization of the random variable as a time series. In summary, ensemble-averaged statistics are obtained as if we observe the physical quantity among a number of identical experiments, while time-averaged statistics are obtained by sampling the physical quantity in a single trial at a uniform temporal interval. The $P(v, t)$ in the FPE is an ensemble-averaged statistic and represents the probability density of having the value v at time t, whereas the empirical TEX law of Thingbaijam and Mai and the distribution of synthetic slip velocities demonstrated in Fig. 4 are time-averaged statistics since the data for calculating the distribution are sampled from one realization (or one earthquake). Generally, the ensemble-averaged statistics and the time-averaged statistics give disparate results since they are calculated in fundamentally different ways; in the cases where the ensemble-averaged statistics of samples at $t \to \infty$ always equal the time-averaged statistics of a sample path of infinite length, the stochastic process is said to be ergodic (Coffey et al., 1996; Gray, 2009; Pavliotis, 2014; Von Plato, 1991). Ergodicity of a dynamical system means that almost all possible states should have been visited and every state is recurrent in a sample path that is sufficiently long. Since the steady-state solution of the FPE (Eq. 6) is unique and its total integral converges, mathematically the proposed stochastic process of Coulomb friction (with $F_C > F_{\text{ext}}$) is ergodic according to the ergodic theorem (Gray, 2009; Pavliotis, 2014). As a consequence of ergodicity, if a sample path is sufficiently long that the contribution due to different initial conditions to the time-averaged statistics is negligible, the average statistical properties of the dynamical system can be deduced from this single sample path. The ergodic nature of the stochastic process of Coulomb friction explains the fact that the time-averaged slip distributions also effectively fit the TEX or EXP model. Accordingly, we can better understand the results of the numerical simulations demonstrated in Fig. 4. For the sample paths of longer durations, the distribution of synthetic velocities generally fits either the EXP or the TEX model better, and the best-fitting parameter v_c better approximates the theoretical expectation calculated from the steady-state solution (47.5 for $D = 5,\ F_C = 1$, and $F_{\text{ext}} = 0.9$ according to Eq. 14). In summary, for a dynamical system that is not allowed to run for an adequately long time, even though the result may fit either the TEX or the EXP model well, the best-fitting parameter yields little to no useful information. Only when the process possesses sufficient ergodic properties can the scale parameter (v_c) of the empirical distribution of rupture slips be formulated according to the level of background noise (D), the driving force (F_{ext}) and the dissipation rate (F_C).

The presence of a single characteristic timescale follows directly from our model's assumptions, which coarse-grain over spatially varying properties of the fault system and assume additive, memoryless noise. This framework naturally produces velocity statistics with exponential-like tails, consistent with TEX distributions reported for spatial final-slip of large earthquakes (Thingbaijam & Mai, 2016). As we treat the local slip duration T as a random variable, the process can be modeled as a Markov diffusion that terminates when slip is arrested at an absorbing boundary. The survival probability $S(t)$ (the probability the process has not been arrested by time t) is asymptotically exponential for long durations:

$$S(t) \sim e^{-\lambda t} \quad \text{as} \quad t \to \infty, \tag{22}$$

where λ is the spectral gap (the smallest nonzero eigenvalue) of the system's Fokker–Planck operator, with $\lambda \approx \kappa 2\pi f_c$ and $\kappa = O(1)$. If the slip duration is truncated at a maximum $T_{\max}$, and the final slip is approximated by $U = \bar{v}T$ for a mean slip rate $\bar{v}$, then U follows a TEX distribution:

$$\Pr(U > u) = \Pr\left(T > \frac{u}{\bar{v}}\right) \approx \exp\left(-\lambda \frac{u}{\bar{v}}\right) \quad \text{for} \quad u < u_{\max}, \tag{23}$$

with a cutoff $u_{\max} = \bar{v}T_{\max}$. In Sect. 4.1, the steady-state velocity PDF (Eq. 9) implies a one-sided exponential tail for $v > 0$ with velocity scale $v_c \equiv -D/(F_{\text{ext}} - F_C) = D/(F_C - F_{\text{ext}})$ for $F_{\text{ext}} > 0$. Combining this with the exact mean velocity (Eq. 12) by equating $\bar{v}$ with $\langle v \rangle$ gives $\bar{v}/v_c = 2\rho/(1+\rho)$, so under near-critical loading ($\rho \to 1$) we have $\bar{v} \approx v_c$. Substituting into $u_c = \bar{v}/\lambda$ with $\lambda \approx \kappa 2\pi f_c$ (and using Eq. 20 for f_c) gives the practical mapping

$$u_c \approx \frac{v_c}{\kappa 2\pi f_c}, \qquad u_{\max} \approx v_c T_{\max}. \tag{24}$$

Thus, the TEX parameters inferred from slip are jointly controlled by the velocity scale v_c (determined by Coulomb friction and loading via Eq. 9) and by the spectral relaxation timescale f_c characterized here, which demonstrates consistency between the distributional probability result and the spectral analysis. The exponential tail in Eq. 22 arises because, after an initial transient, the survival probability is dominated by the slowest-decaying mode of the system. This exponential form of event survival in time has a spatial analog in mapped surface ruptures, where the cumulative event likelihood versus rupture length is reasonably modeled as an exponential decay based on field mapping (Rodriguez Padilla et al., 2024). By contrast, the TEX model for coseismic slip is inferred from finite-fault inversions of kinematic rupture models (Thingbaijam & Mai, 2016). Although earthquake dynamics are complex, the coarse-graining inherent in seismological inversions often smooths high-frequency spatial and temporal variations, plausibly producing an effective local process with a dominant single slow relaxation mode. If that is the case, our model offers a physical interpretation for the TEX parameters: the scale parameter u_c and cutoff $u_{\max}$ are controlled by the corner frequency f_c, the mean slip rate $\bar{v}$, and the maximum slip duration $T_{\max}$. A rigorous connection would, however, require a formal mapping from the temporal velocity process of this zero-dimensional model to the final spatial slip distribution.

5.4. Implication to the Concept of Earthquake Quanta

The representative Brownian particle for an earthquake in this study is very similar in concept to the seismon, which instantiates the seismic source as imaginary particles proposed by Wu et al. (1996). Wu et al. (1996) defined an earthquake quantum as a basic elementary earthquake event composed of seismons, which are quasi-particles similar to the phonon in solid-state physics; accordingly, the statistical properties of an earthquake phenomenon can be obtained through thermodynamic approaches. However, in discussing the physical significance of the representative Brownian particle, we adopt a different interpretation from that of Wu et al. (1996). Wu et al. (1996) regarded the near-equilibrium problem of a "seismon gas" as a simplification of the earthquake source process at the timescale of only the occurrence of the mainshock. Thus, the scope of their model does not include the initiation/stopping mechanism, and shear slips are supposed to equally favor all directions. In this study, by regarding earthquake phenomena as transient frictional instabilities during the steady-state stochastic process of Coulomb friction, we simplify the problem of a tectonic process as a problem of Brownian particles in thermal equilibrium. The representative Brownian particle as the earthquake quantum allows statistical description of the mechanics of an infinitely extended slider-block system driven by an external constant force (F_{ext} in Eq. 1) with Coulomb friction damping (F_C in Eq. 1). The additional F_{ext} term as the driving force naturally causes the simulated rupture slips to prefer a specific direction, allowing a more realistic model for earthquake dynamics to be established. By instantiating earthquake activities as the sample paths of particles in the velocity space, we can generate a discussion in terms of an earthquake event and rupture slip.

5.5. Model Scope and Exclusions from Scale-Free Earthquake Behavior

Our model deliberately simplifies the complexity of a fault system into a coarse-grained, zero-dimensional representation. The constant friction (F_C) and stochastic diffusion (D) are not meant to describe a specific fault patch; instead they serve as mean-field parameters representing the aggregate behavior of a large, heterogeneous tectonic system, which in reality includes features such as self-affine fault roughness that correlates with slip heterogeneity (Candela et al., 2011), discrete geometrical barriers that can arrest rupture (Rodriguez Padilla et al., 2024), and the concentration of slip into asperities with high stress drop (Asano & Iwata, 2011; Somerville et al., 1999). The model seeks to describe the statistical properties of intra-event slip velocity variability under a set of homogeneous, coarse-grained conditions. In its present form it is not intended to reproduce the scale-free behaviors often associated with earthquake physics. Specifically, it does not generate: (1) power-law probability distributions for event sizes or slip, which typically arise from mechanisms such as self-organized criticality or multiplicative noise; (2) a power-law decay regime in its temporal spectrum, which would imply an absence of a characteristic scale; or (3) heterogeneous asperity statistics and self-affine fault roughness, phenomena that require spatially explicit physics. Producing such power-law features would require extending the model to include ingredients like state-dependent (multiplicative) noise, long-range stress transfer, or nonlinear frictional feedback; these are directions for future work.

Despite the above exclusions, the steady-state slip distribution from the FPE can be evaluated against the asperity criterion of Somerville et al. (1999), which defines an asperity as the region where slip exceeds 1.5 times the average slip. Under this exponential slip distribution (see Appendix A.3), a proportion of $\sim 22\%$ (0.223) is predicted to exceed this threshold, falling within the 20–30% range observed empirically by Somerville et al. (1999). Consequently, this top fraction contributes $\sim 56\%$ of the total slip and $\sim 81\%$ of the energy (using squared slip as an upper-bound proxy). These predicted shares align with existing estimates. Somerville et al. (1999) report an average slip share of 44% for asperities from empirical events. Regarding seismic moment, Venegas-Aravena (2023) find that asperity contributions can reach $\sim 73\%$ in kinematic simulations. Unlike finite empirical ruptures, the theoretical distribution originates from the Langevin model that operates on an unbounded state space with infinite duration, permitting arbitrarily large slips and thus elevating the predicted shares especially for energy amplified by squaring. Incorporating finite-domain boundary conditions or self-arrest mechanisms in future extensions would truncate the slip distribution and bring the predicted energy share closer to empirical observations.

6. Conclusion

In the conventional sense, an "earthquake event" denotes a local cluster of asperity failures that are able to be clearly distinguished on the human timescale. By regarding earthquakes as frictional instabilities in the collision of tectonic plates occurring steadily throughout the tectonic timescale, we propose to model the stochastic dynamics of earthquake ruptures by means of the Langevin equation and FPE. The proposed Langevin equation instantiates the earthquake rupture process as the sample path of the representative Brownian particle, with the diffusion term accounting for random collisions and chaotic interactions caused by the highly heterogeneous properties of fault planes. We obtain sample paths by numerically solving the Langevin equation and acquire the analytical distribution of the particle velocity by solving the corresponding FPE with the steady-state approximation. Spectral analysis of the velocity fluctuations reveals single-corner Lorentzian behavior, with the corner frequency controlled by the balance between frictional dissipation and external driving. By regarding an event as a macroscopic slip session and considering local slips as the displacements in each microscopic step of the sample path, we can discuss the energy–duration relationship and the empirical distribution of the rupture slips of earthquakes based on both the numerical and the analytical results. Regarding the slip distribution, we demonstrate that numerically obtained samples generally follow the TEX model, which is obtained empirically based on the source model of large events worldwide. The FPE solution is generally a double-sided EXP function; however, for a process of finite duration with a large F_{ext}/F_C ratio that particularly favors the generation of large synthetic events, the FPE solution approximates the TEX model. This suggests a connection between the physical parameters in the Langevin equation and the scale parameter in the TEX model. The characteristic timescale revealed by spectral analysis provides a physical basis for understanding why slip distributions inferred from finite-source inversions follow exponential-like forms, as the single dominant relaxation mode governs the survival probability of ongoing slip events. Concerning the energy–duration relationship, a nearly constant scaling exponent of $n = 2/3$ for the power law $T \propto E_{\text{diss}}^n$ is observed among groups of events simulated with a broad range of physical parameters, suggesting a consistent energy–duration scaling within the additive-noise, Coulomb-damping framework. Although the $T \propto E_{\text{diss}}^{2/3}$ proportionality obtained in this study is different from the most common scaling of $T \propto M_0^{1/3}$ for general earthquake ruptures, the discrepancy may be attributed to the differences in the dimensionality of the model and the criteria for defining an event. However, it should be noted that the moment is not equivalent to energy, and the obtained $E_{\text{diss}} - T$ relationship depends solely on the numerically simulated results; further research must be conducted to discuss this topic in greater depth. Different versions of the Langevin equation have been adopted to investigate the dynamics of large many-body systems, for example, to predict the evolution of a vibrated granular system (Hayakawa, 2005), to simulate the friction process at the nanoscale (Vanossi et al., 2013), and to establish a framework for earthquake dynamics (Ide, 2008; Ide & Yabe, 2019; Rundle et al., 1996). With regard to earthquake dynamics, the Brownian walk model proposed by Ide (2008) for slow earthquakes and the traveling density wave model of Rundle et al. (1996) describe an earthquake rupture as a kind of stochastic process. Ide applied a typical Langevin equation with viscous damping to the rupture process of slow earthquakes by defining the overall rupture area as the random variable. For the traveling density wave model, in which a Langevin equation with a periodically changing force is applied to reproduce the quasi-periodical behavior of earthquake occurrence, Rundle et al. regarded an earthquake event as a sudden transition toward the minimal free energy of the fault system. Like these studies, this study successfully simplifies the highly complex problem of earthquake dynamics by means of Langevin's approach; thus, similar to the Brownian walk model and the traveling density wave model, our model is capable of producing scaling laws similar to empirically observed ruptures. As our model is idealized and deliberately coarse-grained, several discrepancies between the physical meaning of our model and real scenarios should be noted. First, collisions or any other kinds of force interactions in a real seismogenic process have memory effects, but the interaction time in this study is assumed to be infinitesimal. Second, the simulated source processes in this study can differ considerably from a conventional earthquake. Whereas in a conventional earthquake rupture branches and develops asynchronously, our model limits rupture slip to take place consecutively one-by-one. Furthermore, under the white-noise closure the effective velocity process is Markovian; in reality ruptures may exhibit spatial correlations arising from stress transfer, evolving friction, and geometry. Finally, our formulation is spatially 0-D and 1-D in state space (a single-degree-of-freedom model), whereas the ruptures of real earthquakes evolve in a space of two or more dimensions. Despite these limitations, the model successfully represents aggregate behavior of a heterogeneous tectonic system through mean-field parameters. In the future, as this model is capable of reproducing source processes directly in the velocity space, additional insights into the scaling laws of seismology and statistical properties of earthquakes will be obtained. Moreover, the Langevin equation of Coulomb friction can be further generalized to fit more complex scenarios. For example, the Langevin equation can be dimensionally extended to simulate earthquake ruptures in two-dimensional space, and a periodical external force can be employed for seismic hazard assessments. Developments in probabilistic tsunami and seismic hazard assessments have also included the stochastic slip distributions of earthquakes to determine the overall probability distributions of particular tsunami heights or ground shaking levels [e.g., Geist and Parsons (2006, 2009)]. Stochastic slip models quantify variations in slip to reasonably estimate the probability of a specified tsunami height or ground shaking intensity at an individual location resulting from a specific fault.

Acknowledgements

We would like to sincerely thank Prof. Jeen-Hwa Wang (Institute of Earth Sciences, Academia Sinica) for his substantial contribution to this work. His insightful comments greatly improved the quality of our research, and we are grateful for his valuable input and guidance throughout the revision of this manuscript. For select portions of this manuscript, the authors utilized AI-powered tools to assist with copy editing and enhance readability. All authors have reviewed the final text to ensure it accurately reflects their original work and take full responsibility for the manuscript's content.

Author Contributions T.-H. Wu and C.-C. Chen contributed to this work as follows: T.-H. Wu wrote the main manuscript text and contributed to experimental design, literature review, data analysis, visualization, methodology development, and software or tool development. C.-C. Chen was involved in project administration, conceptualization of the study, methodology development, supervision of the research, and provided critical review and critique. All authors reviewed the manuscript.

Funding

This work was supported by the National Science and Technology Council (NSTC), Taiwan, under Grant Numbers NSTC 113-2116-M-008-016-MY3 and NSTC 114-2811-M-008-061.

Data Availability

The data underlying this article will be shared on reasonable request to the corresponding author.

Declarations

Conflict of interest The authors declare no Conflict of interest.

Appendix A

A.1 Derivations of the Single-Corner Amplitude Spectrum for Coulomb-Friction SDE

This appendix derives the single-corner amplitude spectrum model for the Coulomb-friction Langevin process used to fit the sample paths in Fig. 7.

(1) Process and effective potential.

Consider the 1-D stochastic differential equation (SDE)

$$\mathrm{d}v(t) = -F_C \frac{v(t)}{|v(t)|}\mathrm{d}t + F_{\text{ext}}\mathrm{d}t + \sqrt{2D}\mathrm{d}W(t), \quad \text{(A1)}$$

with additive white noise of strength D and constants $F_C > 0$, F_{ext}. For $v \neq 0$, the drift is $A(v) = -F_C \mathrm{sign}(v) + F_{\text{ext}}$. In an overdamped Langevin form, $A(v) = -\partial_v U(v)$, which yields the V-shaped effective potential

$$U(v) = F_C|v| - F_{\text{ext}}v. \quad \text{(A2)}$$

When $|F_{\text{ext}}| < F_C$, the steady density is well defined and piecewise exponential: $p_s(v) \propto e^{-U(v)/D}$.

(2) Single-pole relaxation.

The Fokker–Planck operator associated with Eq. A1 has a spectral gap for $|F_{\text{ext}}| < F_C$. Consequently, the centered velocity $g(v) = v - \langle v \rangle$ relaxes approximately as a single mode after a short transient,

$$C_v(t) \equiv \mathrm{Cov}\left[v(t), v(0)\right] \approx \sigma_v^2 e^{-|t|/\tau}, \quad \text{(A3)}$$

with variance σ_v^2 under p_s and correlation time $\tau > 0$ (the inverse of the smallest nonzero eigenvalue).

(3) Lorentzian PSD and its square root.

The two-sided power spectral density (PSD) with respect to angular frequency ω is the Fourier transform of C_v:

$$S_{vv}^{(\omega)}(\omega) = \int_{-\infty}^{\infty} C_v(t) e^{-i\omega t}\mathrm{d}t = \frac{2\sigma_v^2 \tau}{1 + (\omega\tau)^2}. \quad \text{(A4)}$$

The amplitude spectral density (ASD) with respect to ω is

$$S_v^{(\omega)}(\omega) = \sqrt{S_{vv}^{(\omega)}(\omega)} = \frac{\sqrt{2\sigma_v^2\tau}}{\sqrt{1 + (\omega/\omega_c)^2}}, \quad \omega_c \equiv \tau^{-1}. \quad \text{(A5)}$$

(4) Converting to frequency

f (Hz). Let $\omega = 2\pi f$ and denote the PSD/ASD per Hz by $S_{vv}^{(f)}(f)$ and $S_v^{(f)}(f)$. Because $\mathrm{d}\omega = 2\pi \mathrm{d}f$ and variances are invariant under change of variable, we have

$$S_{vv}^{(f)}(f) = S_{vv}^{(\omega)}(2\pi f) = \frac{2\sigma_v^2\tau}{1 + \left(2\pi f \tau\right)^2} = \frac{2\sigma_v^2\tau}{1 + (f/f_c)^2}, \quad f_c \equiv \frac{1}{2\pi\tau}. \quad \text{(A6)}$$

Taking the square root gives the ASD form used in our fits (the amplitude spectrum in Hz):

$$S_v^{(f)}(f) = \frac{S_v^{(f)}(0)}{\sqrt{1 + (f/f_c)^2}}, S_v^{(f)}(0) = \sqrt{S_{vv}^{(f)}(0)} = \sqrt{2\sigma_v^2\tau}. \quad \text{(A7)}$$

This is the frequency-domain (Hz) counterpart of the angular-frequency form $S_v(\omega) = S_v(0)/\sqrt{1 + (\omega/\omega_c)^2}$.

A.2 Edge-Rate Argument and the $g(\rho)$ Form

Define the load ratio $\rho = F_{\mathrm{ext}}/F_C$. Use the dimensionless corner definitions

$$\tilde{f}_c \equiv \frac{f_c D}{F_C^2}, \qquad \tilde{\omega}_c \equiv \frac{\omega_c D}{F_C^2} = 2\pi \tilde{f}_c, \quad (\omega = 2\pi f). \tag{A8}$$

(1) Edge (continuum) rate.

Let $v = V_c \tilde{v}$ and $t = T_c \tilde{t}$ so that $\mathrm{d}W_t = \sqrt{T_c}\mathrm{d}W_{\tilde{t}}$, Eq. A1 becomes

$$\mathrm{d}\tilde{v} = \left[-(F_C T_c/V_c)\mathrm{sign}(\tilde{v}) + (F_{\mathrm{ext}} T_c/V_c) \right]\mathrm{d}\tilde{t} + \frac{\sqrt{2DT_c}}{V_c}\mathrm{d}W_{\tilde{t}}. \tag{A9}$$

Choosing $V_c = D/F_C$ and $T_c = D/F_C^2$ makes $F_C T_c/V_c = 1$ and $\sqrt{2DT_c}/V_c = \sqrt{2}$. With $\rho = F_{\mathrm{ext}}/F_C$, the SDE is non-dimensionalized by $\tilde{v} = \frac{F_C}{D}v$, $\tilde{t} = \frac{F_C^2}{D}t$ as

$$\mathrm{d}\tilde{v} = \left[-\mathrm{sign}(\tilde{v}) + \rho \right]\mathrm{d}\tilde{t} + \sqrt{2}\mathrm{d}W_{\tilde{t}} \tag{A10}$$

The solution to the Fokker-Planck equation can be written as a sum of decaying modes:

$$P(v,t) = \underbrace{c_0 \psi_0(v)\sqrt{p_s(v)}}_{\text{Term for } \lambda_0 = 0} + \underbrace{c_1 e^{-\lambda_1 t}\psi_1(v)\sqrt{p_s(v)}}_{\text{Term for } \lambda_1 \text{ the slowest decaying rate}} + c_2 e^{-\lambda_2 t}\psi_2(v)\sqrt{p_s(v)} + \ldots \tag{A11}$$

The symmetric (Schrödinger-type) operator has a continuous spectrum starting at the lower plateau; the edge gives the slowest nonzero decay rate. With $p_s(v) \propto \exp(-U(v)/D) = \exp(-(|\tilde{v}| - \rho\tilde{v}))$ referring to Eq. A2, the dimensionless effective potential is given as $U(\tilde{v}) = |\tilde{v}| - \rho\tilde{v}$, and the self-adjoint transform of the backward generator gives

$$\mathcal{H}\psi = -\psi'' + V(\tilde{v})\psi, \qquad V(\tilde{v}) = \frac{1}{4}\left[U'(\tilde{v})\right]^2 - \frac{1}{2}U''(\tilde{v}). \tag{A12}$$

Since $U'(\tilde{v}) = 1 - \rho$ for $\tilde{v} > 0$ and $U'(\tilde{v}) = -1 - \rho$ for $\tilde{v} < 0$, and $U'' = 2\delta(\tilde{v})$, we obtain

$$V(\tilde{v}) = \begin{cases} \frac{1}{4}(1-\rho)^2, & \tilde{v} > 0, \\ \frac{1}{4}(1+\rho)^2, & \tilde{v} < 0, \end{cases} \quad \text{with a } -\delta(\tilde{v}) \text{ at } \tilde{v} = 0. \tag{A13}$$

The ground state is at $\tilde{\lambda}_0 = 0$ (stationary density). Above it, the spectrum is continuous and starts at the lower plateau, $\min\{\frac{1}{4}(1-\rho)^2, \frac{1}{4}(1+\rho)^2\} = \frac{1}{4}(1-\rho)^2$ for $\rho \geq 0$. This sets the slowest nonzero decay rate

$$\tilde{\omega}_{c,edge}(\rho) = \frac{(1-\rho)^2}{4}, \qquad 0 \leq \rho < 1. \tag{A14}$$

Using Eq. A8, the dimensionless corner in Hz is

$$\boxed{\tilde{f}_{c,edge}(\rho) = \frac{\tilde{\omega}_{c,edge}}{2\pi} = \frac{(1-\rho)^2}{8\pi}}. \tag{A15}$$

(2) Corner in terms of $g(\rho)$.

From Eq. A14, $\omega_c = (F_C^2/D)\frac{(1-\rho)^2}{4}$. Factor $F_C^2(1-\rho)^2/4$ as $g(\rho)F_C^2(1-\rho^2)$ with

$$g(\rho) = \frac{1-\rho}{4(1+\rho)}, \qquad F_C^2(1-\rho^2) = F_C^2 - F_{\mathrm{ext}}^2. \tag{A16}$$

Therefore

$$\boxed{f_c = \frac{g(\rho)\left(F_C^2 - F_{\mathrm{ext}}^2\right)}{2\pi D}}, \tag{A17}$$

which is equivalent to Eq. A15 after converting between ω and f and using $\rho = F_{\mathrm{ext}}/F_C$.

A.3 Appendix: Mathematical Derivation of Energy Concentration

This appendix derives the slip and energy shares for patches exceeding the asperity threshold ($t_p/\mu = 1.5$), as discussed in Sect. 5.5. Under an exponential slip distribution, we calculate the fraction of fault area exceeding this threshold and the corresponding contributions to total slip and energy. The physical motivation for using S^2 as an energy proxy comes from a simple spring-slider model: if local resistance grows with slip as $F \approx kS$ (elastic loading/reloading), the work (energy released) at that patch is $\int F\mathrm{d}S \approx (1/2)kS^2$, giving energy $\propto S^2$. In contrast, constant dynamic friction yields energy $\propto S$. Real faults likely lie between these limits; S^2 provides an upper-bound proxy for energy concentration in high-slip patches.

Definitions and Assumptions

Consider a fault discretized into N equal-area patches, each experiencing final slip $S_i \geq 0$. We sort patches from largest to smallest slip and define the "top p fraction (by area)" as the first p proportion of patches in the sorted list.

For exponential slip distribution with mean μ:

$$f(s) = \frac{1}{\mu}\exp\left(\frac{-s}{\mu}\right), \quad s \geq 0. \tag{A18}$$

The cumulative distribution function (CDF) is:

$$\mathrm{CDF} = \int_{s=0}^{t} f(s)ds = 1 - \exp\left(\frac{-t}{\mu}\right). \tag{A19}$$

The complementary CDF (tail probability, CCDF) is:

$$P(S > t) = \exp\left(\frac{-t}{\mu}\right). \tag{A20}$$

Threshold Calculation

For the top p fraction, we need the threshold t_p such that $P(S > t_p) = p$:

$$\exp\left(\frac{-t_p}{\mu}\right) = p. \tag{A21}$$

Solving for t_p:

$$t_p = -\mu \ln p. \tag{A22}$$

Expected Values and Integrals

The expected slip per patch is:

$$\mathbb{E}[S] = \mu. \tag{A23}$$

The expected S^2 per patch is:

$$\mathbb{E}[S^2] = 2\mu^2 \tag{A24}$$

For conditional expectations above threshold t, we use the integrals:

$$\mathbb{E}[S; S > t] = \int_t^{\infty} sf(s)ds = (t + \mu)\exp\left(\frac{-t}{\mu}\right), \tag{A25}$$

$$\mathbb{E}[S^2; S > t] = \int_t^{\infty} s^2 f(s)ds = (t^2 + 2\mu t + 2\mu^2)\exp\left(\frac{-t}{\mu}\right). \tag{A26}$$

Slip Share Calculation

The expected slip contributed by patches with $S > t_p$ is:

$$\mathbb{E}[S; S > t_p] = (t_p + \mu)\exp\left(\frac{-t_p}{\mu}\right). \tag{A27}$$

The slip share is:

$$T_S(p) = \frac{\mathbb{E}[S; S > t_p]}{\mathbb{E}[S]} = \frac{(t_p + \mu)\exp(-t_p/\mu)}{\mu}. \tag{A28}$$

Substituting $t_p = -\mu \ln p$ and $\exp(-t_p/\mu) = p$:

$$T_S(p) = \frac{(-\mu \ln p + \mu)p}{\mu} = p(1 - \ln p). \tag{A29}$$

Energy Share Calculation

The expected S^2 contributed by patches with $S > t_p$ is:

$$\mathbb{E}[S^2; S > t_p] = (t_p^2 + 2\mu t_p + 2\mu^2)\exp\left(\frac{-t_p}{\mu}\right). \tag{A30}$$

The energy share is:

$$T_{S^2}(p) = \frac{\mathbb{E}[S^2; S > t_p]}{\mathbb{E}[S^2]} = \frac{(t_p^2 + 2\mu t_p + 2\mu^2)\exp(-t_p/\mu)}{2\mu^2}. \tag{A31}$$

Substituting $t_p = -\mu \ln p$:

$$T_{S^2}(p) = \frac{p}{2}\left[(\ln(1/p) + 1)^2 + 1\right]. \tag{A32}$$

Numerical Examples

The table below lists slip and energy shares for several threshold values. The bolded row corresponds to the asperity threshold $t_p/\mu = 1.5$.

Threshold t_p/μ	p	Slip share $T_{S^1}(p)$	Energy share $T_{S^2}(p)$
2.3	0.1	0.3303 (≈ 33 %)	0.5954 (≈ 60 %)
1.6	0.2	0.5219 (≈ 52 %)	0.7809 (≈ 78 %)
1.5	**0.223**	**0.5578** (≈ **56** %)	**0.8088** (≈ **81** %)
1.2	0.3	0.6612 (≈ 66 %)	0.8786 (≈ 88 %)
0.92	0.4	0.7665 (≈ 77 %)	0.9344 (≈ 93 %)

Publisher's Note Springer Nature remains neutral with regard to jurisdictional claims in published maps and institutional affiliations.

References

Adjemian, F., & Evesque, P. (2004). Experimental study of stick-slip behaviour. *International Journal for Numerical and Analytical Methods in Geomechanics, 28*(6), 501–530. https://doi.org/10.1002/nag.350

Aguiar, A. C., Melbourne, T. I., & Scrivner, C. W. (2009). Moment release rate of Cascadia tremor constrained by GPS. *Journal of Geophysical Research: Solid Earth*. https://doi.org/10.1029/2008JB005909

Aki, K. (1972). Earthquake mechanism. *Tectonophysics, 13*(1), 423–446. https://doi.org/10.1016/0040-1951(72)90032-7

Aki, K. (1979). Characterization of barriers on an earthquake fault. *Journal of Geophysical Research: Solid Earth, 84*(B11), 6140–6148. https://doi.org/10.1029/JB084iB11p06140

Aki, K. (1984). Asperities, barriers, characteristic earthquakes and strong motion prediction. *Journal of Geophysical Research: Solid Earth*. https://doi.org/10.1029/JB089IB07P05867

Aki, K. (1987). Magnitude-frequency relation for small earthquakes: A clue to the origin of *f*max of large earthquakes. *Journal of Geophysical Research: Solid Earth, 92*(B2), 1349–1355. https://doi.org/10.1029/JB092iB02p01349

Albertini, G., Karrer, S., Grigoriu, M. D., & Kammer, D. S. (2020). Stochastic properties of static friction. *Journal of the Mechanics and Physics of Solids, 147*, Article 104242. https://doi.org/10.1016/j.jmps.2020.104242

Asano, K., & Iwata, T. (2011). Characterization of stress drops on asperities estimated from the heterogeneous kinematic slip model for strong motion prediction for Inland Crustal earthquakes in Japan. *Pure and Applied Geophysics, 168*(1), 105–116. https://doi.org/10.1007/s00024-010-0116-y

Aviles, C. A., Scholz, C. H., & Boatwright, J. (1987). Fractal analysis applied to characteristic segments of the San Andreas Fault. *Journal of Geophysical Research: Solid Earth, 92*(B1), 331–344. https://doi.org/10.1029/JB092iB01p00331

Bak, P., Christensen, K., Danon, L., & Scanlon, T. (2002). Unified scaling law for earthquakes. *Physical Review Letters, 88*(17), Article 178501. https://doi.org/10.1103/PhysRevLett.88.178501

Brace, W. F., & Byerlee, J. D. (1966). Stick-slip as a mechanism for earthquakes. *Science, 153*(3739), 990–992. https://doi.org/10.1126/science.153.3739.990

Brown, S. R., & Scholz, C. H. (1985). Closure of random elastic surfaces in contact. *Journal of Geophysical Research: Solid Earth, 90*(B7), 5531–5545. https://doi.org/10.1029/JB090iB07p05531

Brown, S. R., & Scholz, C. H. (1985). Broad bandwidth study of the topography of natural rock surfaces. *Journal of Geophysical Research: Solid Earth, 90*(B14), 12575–12582. https://doi.org/10.1029/JB090iB14p12575

Burridge, R., & Knopoff, L. (1967). Model and theoretical seismicity. *Bulletin of the Seismological Society of America, 57*(3), 341–371.

Byerlee, J. D. (1967). Frictional characteristics of granite under high confining pressure. *Journal of Geophysical Research, 72*(14), 3639–3648. https://doi.org/10.1029/JZ072i014p03639

Candela, T., Renard, F., Schmittbuhl, J., Bouchon, M., & Brodsky, E. E. (2011). Fault slip distribution and fault roughness. *Geophysical Journal International, 187*(2), 959–968. https://doi.org/10.1111/j.1365-246X.2011.05189.x

Carpinteri, A., & Paggi, M. (2009). A fractal interpretation of size-scale effects on strength, friction and fracture energy of faults. *Chaos, Solitons and Fractals, 39*(2), 540–546.

Coffey, W. T., Kalmykov, Y. P., & Waldron, J. T. (1996). *The Langevin equation: With applications in physics, chemistry and electrical engineering* World Scientific series in contemporary chemical physics (Vol. 10). Singapore: World Scientific.

Costamagna, R., Renner, J., & Bruhns, O. T. (2007). Relationship between fracture and friction for brittle rocks. *Mechanics of Materials, 39*(4), 291–301. https://doi.org/10.1016/j.mechmat.2006.06.001

Cyganowski, S., Kloeden, P., & Ombach, J. (2001). *From elementary probability to stochastic differential equations with MAPLE®*. Berlin: Springer Science & Business Media.

de Wit, C. C., Olsson, H., Astrom, K. J., & Lischinsky, P. (1995). A new model for control of systems with friction. *IEEE Transactions on Automatic Control, 40*(3), 419–425. https://doi.org/10.1109/9.376053

Eckmann, J.-P. (1981). Roads to turbulence in dissipative dynamical systems. *Reviews of Modern Physics, 53*(4), 643–654. https://doi.org/10.1103/RevModPhys.53.643

Einstein, A. (2003). *Investigation on the theory of the Brownian movement*. Mineola: Dover.

Frank, W. B., Rousset, B., Lasserre, C., & Campillo, M. (2018). Revealing the cluster of slow transients behind a large slow slip event. *Science Advances, 4*(5), 0661. https://doi.org/10.1126/sciadv.aat0661

Furumoto, M., & Nakanishi, I. (1983). Source times and scaling relations of large earthquakes. *Journal of Geophysical Research: Solid Earth, 88*(B3), 2191–2198. https://doi.org/10.1029/JB088iB03p02191

Gao, H., Schmidt, D. A., & Weldon, R. J. (2012). Scaling relationships of source parameters for slow slip EventsScaling relationships of source parameters for slow slip events. *Bulletin of the Seismological Society of America, 102*(1), 352–360. https://doi.org/10.1785/0120110096

Gardiner, C. W. (2004). *Handbook of stochastic methods for physics, chemistry, and the natural sciences* Springer series in synergetics (2nd ed.). Berlin: Springer.

Geist, E. L., & Parsons, T. (2006). Probabilistic analysis of Tsunami hazards. *Natural Hazards, 37*(3), 277–314. https://doi.org/10.1007/s11069-005-4646-z

Geist, E. L., & Parsons, T. (2009). Assessment of source probabilities for potential tsunamis affecting the U.S. Atlantic coast. *Marine Geology, 264*(1–2), 11. https://doi.org/10.1016/j.margeo.2008.08.005

Geller, R. J. (1976). Scaling relations for earthquake source parameters and magnitudes. *Bulletin of the Seismological Society of America, 66*(5), 1501–1523.

Goebel, T. H. W., Sammis, C. G., Becker, T. W., Dresen, G., & Schorlemmer, D. (2015). A comparison of seismicity characteristics and fault structure between stick-slip experiments and nature. *Pure and Applied Geophysics, 172*(8), 2247–2264. https://doi.org/10.1007/s00024-013-0713-7

Gomberg, J., Wech, A., Creager, K., Obara, K., & Agnew, D. (2016). Reconsidering earthquake scaling. *Geophysical Research Letters, 43*(12), 6243–6251. https://doi.org/10.1002/2016GL069967

Gray, R. M. (2009). Ergodic theorems. In R. M. Gray (Ed.), *Probability, random processes, and ergodic properties* (pp. 239–262). Boston: Springer. https://doi.org/10.1007/978-1-4419-1090-5_8

Gross, S.J.(2000). Traveling wave and rough fault earthquake models: Illuminating the relationship between slip deficit and event frequency statistics. In: Rundle, J. B., Turcotte, D. L., Klein, W. (Eds.) Geocomplexity and the physics of earthquakes. Geophysical monograph series, vol. 120, pp. 73–82. American Geophysical Union, Washington, DC . https://doi.org/10.1029/GM120p0073

Haessig, D. A., & Friedland, B. (1991). On the modeling and simulation of friction. *Journal of Dynamic Systems, Measurement, and Control, 113*(3), 354–362. https://doi.org/10.1115/1.2896418

Hänggi, P., & Marchesoni, F. (2005). Introduction: 100years of Brownian motion. *Chaos: An Interdisciplinary Journal of Nonlinear Science, 15*(2), Article 026101. https://doi.org/10.1063/1.1895505

Hayakawa, H. (2005). Langevin equation with Coulomb friction. *Physica D: Nonlinear Phenomena, 205*(1–4), 48–56. https://doi.org/10.1016/j.physd.2004.12.011

Houston, H. (2001). Influence of depth, focal mechanism, and tectonic setting on the shape and duration of earthquake source time functions. *Journal of Geophysical Research: Solid Earth, 106*(B6), 11137–11150. https://doi.org/10.1029/2000JB900468

Huang, J., & Turcotte, D. L. (1990). Are earthquakes an example of deterministic chaos? *Geophysical Research Letters, 17*(3), 223–226. https://doi.org/10.1029/GL017i003p00223

Huang, J., & Turcotte, D. L. (1992). Chaotic seismic faulting with a mass-spring model and velocity-weakening friction. *Pure and Applied Geophysics, 138*(4), 569–589. https://doi.org/10.1007/BF00876339

Ide, S. (2008). A Brownian walk model for slow earthquakes. *Geophysical Research Letters, 35*(17), 17301. https://doi.org/10.1029/2008GL034821

Ide, S., Beroza, G. C., Shelly, D. R., & Uchide, T. (2007). A scaling law for slow earthquakes. *Nature, 447*(7140), 76–79. https://doi.org/10.1038/nature05780

Ide, S., Imanishi, K., Yoshida, Y., Beroza, G. C., & Shelly, D. R. (2008). Bridging the gap between seismically and geodetically detected slow earthquakes. *Geophysical Research Letters*. https://doi.org/10.1029/2008GL034014

Ide, S., & Yabe, S. (2019). Two-dimensional probabilistic cell automaton model for broadband slow earthquakes. *Pure and Applied Geophysics, 176*(3), 1021–1036. https://doi.org/10.1007/s00024-018-1976-9

Jazwinski, A. H. (1970). *Stochastic processes and filtering theory*. New York: Academic Press.

Kagan, Y. Y. (1997). Are earthquakes predictable? *Geophysical Journal International, 131*(3), 505–525. https://doi.org/10.1111/j.1365-246X.1997.tb06595.x

Kampen, N. G. (1981). *Stochastic processes in physics and chemistry*. Amsterdam: North-Holland.

Kanamori, H., & Anderson, D. L. (1975). Theoretical basis of some empirical relations in seismology. *Bulletin of the Seismological Society of America, 65*(5), 1073–1095.

Kanamori, H., & Stewart, G. S. (1978). Seismological aspects of the Guatemala Earthquake of February 4, 1976. *Journal of Geophysical Research: Solid Earth, 83*(B7), 3427–3434. https://doi.org/10.1029/JB083iB07p03427

Kaproth, B. M., & Marone, C. (2013). Slow earthquakes, preseismic velocity changes, and the origin of slow frictional stick-slip. *Science, 341*(6151), 1229–1232. https://doi.org/10.1126/science.1239577

Kubo, R. (1966). The fluctuation-dissipation theorem. *Reports on Progress in Physics, 29*, 255–284. https://doi.org/10.1088/0034-4885/29/1/306

Labuz, J. F., & Zang, A. (2012). Mohr-Coulomb failure criterion. *Rock Mechanics and Rock Engineering, 45*(6), 975–979. https://doi.org/10.1007/s00603-012-0281-7

Lavallée, D., Liu, P., & Archuleta, R. J. (2006). Stochastic model of heterogeneity in earthquake slip spatial distributions. *Geophysical Journal International, 165*(2), 622–640. https://doi.org/10.1111/j.1365-246X.2006.02943.x

Legrand, D. (2002). Fractal dimensions of small, intermediate, and large earthquakes. *Bulletin of the Seismological Society of America, 92*(8), 3318–3320. https://doi.org/10.1785/0120020025

Lemons, D.S., Gythiel, A.: Paul Langevin's 1908 paper On the theory of Brownian motion ["Sur la théorie du mouvement brownien," C. R. Acad. Sci. (Paris) 146, 530–533 (1908)]. American Journal of Physics 65(11), 1079–1081 (1997) https://doi.org/10.1119/1.18725

Liang, J., Fillmore, S., & Ma, O. (2012). An extended bristle friction force model with experimental validation. *Mechanism and Machine Theory, 56*, 123–137. https://doi.org/10.1016/j.mechmachtheory.2012.06.002

Mai, P. M., & Beroza, G. C. (2002). A spatial random field model to characterize complexity in earthquake slip. *Journal of Geophysical Research: Solid Earth, 107*(B11), 10–11021. https://doi.org/10.1029/2001JB000588

Michel, S., Gualandi, A., & Avouac, J.-P. (2019). Similar scaling laws for earthquakes and Cascadia slow-slip events. *Nature, 574*(7779), 522–526. https://doi.org/10.1038/s41586-019-1673-6

Moreno-Torres, L. R., Gomez-Vieyra, A., Lovallo, M., Ramírez-Rojas, A., & Telesca, L. (2018). Investigating the interaction between rough surfaces by using the Fisher-Shannon method: Implications on interaction between tectonic plates. *Physica A: Statistical Mechanics and its Applications, 506*, 560–565. https://doi.org/10.1016/j.physa.2018.04.023

Murphy, S., & Herrero, A. (2020). Surface rupture in stochastic slip models. *Geophysical Journal International, 221*(2), 1081–1089. https://doi.org/10.1093/gji/ggaa055

Ohnaka, M., Kuwahara, Y., Yamamoto, K., & Hirasawa, T. (1986). Dynamic breakdown processes and the generating mechanism for high-frequency elastic radiation during stick-slip instabilities. In: Das, S., Boatwright, J., Scholz, C.H. (eds.) Earthquake source mechanics. Geophysical monograph series, pp. 13–24. American Geophysical Union (AGU), Washington, DC . https://doi.org/10.1029/GM037p0013

Ohnaka, M. (2003). A constitutive scaling law and a unified comprehension for frictional slip failure, shear fracture of intact rock, and earthquake rupture. *Journal of Geophysical Research: Solid Earth*. https://doi.org/10.1029/2000JB000123

Ohnaka, M., Akatsu, M., Mochizuki, H., Odedra, A., Tagashira, F., & Yamamoto, Y. (1997). A constitutive law for the shear failure of rock under lithospheric conditions. *Tectonophysics, 277*(1), 1–27. https://doi.org/10.1016/S0040-1951(97)00075-9

Okubo, P. G., & Dieterich, J. H. (1984). Effects of physical fault properties on frictional instabilities produced on simulated faults.

Journal of Geophysical Research: Solid Earth, 89(B7), 5817–5827. https://doi.org/10.1029/JB089iB07p05817

Papageorgiou, A. S., & Aki, K. (1983). A specific barrier model for the quantitative description of inhomogeneous faulting and the prediction of strong ground motion. I. Description of the model. *Bulletin of the Seismological Society of America, 73*(3), 693–722. https://doi.org/10.1785/BSSA0730030693

Pavliotis, G.A. (2014). Stochastic processes and applications: diffusion processes, the Fokker-Planck and Langevin equations. Texts in applied mathematics, vol. 60. Springer, New York, NY . https://doi.org/10.1007/978-1-4939-1323-7

Pavliotis, G.A. (2014). Stochastic processes and applications: Diffusion processes, the Fokker-Planck And Langevin equations. Texts in applied mathematics. Springer-Verlag, New York . https://doi.org/10.1007/978-1-4939-1323-7

Pei, L., Hyun, S., Molinari, J. F., & Robbins, M. O. (2005). Finite element modeling of elasto-plastic contact between rough surfaces. *Journal of the Mechanics and Physics of Solids, 53*(11), 2385–2409. https://doi.org/10.1016/j.jmps.2005.06.008

Renard, F., & Candela, T. (2017). Scaling of fault roughness and implications for earthquake mechanics. In: Thomas, M.Y., Mitchell, T.M., Bhat, H.S. (eds.) Fault zone dynamic processes. Geophysical monograph series, pp 195–215. American Geophysical Union (AGU), Washington, DC . Chap. 10. https://doi.org/10.1002/9781119156895.ch10

Renn, J. (2005). Einstein's invention of Brownian motion. *Annalen der Physik, 14*(S1), 23–37. https://doi.org/10.1002/andp.200410131

Rivera, L., & Kanamori, H. (2002). Spatial heterogeneity of tectonic stress and friction in the crust. *Geophysical Research Letters, 29*(6), 12–1124. https://doi.org/10.1029/2001GL013803

Rodriguez Padilla, A. M., Oskin, M. E., Brodsky, E. E., Dascher-Cousineau, K., Herrera, V., & White, S. (2024). The influence of fault geometrical complexity on surface rupture length. *Geophysical Research Letters, 51*(20), 2024–109957. https://doi.org/10.1029/2024GL109957

Ruina, A. (1983). Slip instability and state variable friction laws. *Journal of Geophysical Research: Solid Earth, 88*(B12), 10359–10370. https://doi.org/10.1029/JB088iB12p10359

Rundle, J. B., Klein, W., & Gross, S. (1996). Dynamics of a traveling density wave model for earthquakes. *Physical Review Letters, 76*(22), 4285–4288. https://doi.org/10.1103/PhysRevLett.76.4285

Rundle, J. B., Turcotte, D. L., Shcherbakov, R., Klein, W., & Sammis, C. (2003). Statistical physics approach to understanding the multiscale dynamics of earthquake fault systems. *Reviews of Geophysics, 41*(4), 1019. https://doi.org/10.1029/2003RG000135

Saltiel, S., Bonner, B. P., Mittal, T., Delbridge, B., & Ajo-Franklin, J. B. (2017). Experimental evidence for dynamic friction on rock fractures from frequency-dependent nonlinear hysteresis and harmonic generation. *Journal of Geophysical Research: Solid Earth, 122*(7), 4982–4999. https://doi.org/10.1002/2017JB014219

Scholz, C. H. (1982). Scaling laws for large earthquakes: Consequences for physical models. *Bulletin of the Seismological Society of America, 72*(1), 1–14.

Scholz, C. H. (1990). *The mechanics of earthquakes and faulting*. Cambridge University Press.

Scholz, C. H., & Aviles, C. A. (1986). Earthquake source mechanics. Geophysical monograph series,. In S. Das, J. Boatwright, & C. H. Scholz (Eds.), (pp. 147–155). American Geophysical Union (AGU). https://doi.org/10.1029/GM037p0147

Somerville, P., Irikura, K., Graves, R., Sawada, S., Wald, D., Abrahamson, N., Iwasaki, Y., Kagawa, T., Smith, N., & Kowada, A. (1999). Characterizing crustal earthquake slip models for the prediction of strong ground motion. *Seismological Research Letters, 70*(1), 59–80. https://doi.org/10.1785/gssrl.70.1.59

Sun, J., Yu, Y., & Li, Y. (2018). Stochastic finite-fault simulation of the 2017 Jiuzhaigou Earthquake in China. *Earth, Planets and Space, 70*(1), 128. https://doi.org/10.1186/s40623-018-0897-2

Tanioka, Y., & Ruff, L. J. (1997). Source time functions. *Seismological Research Letters, 68*(3), 386–400. https://doi.org/10.1785/gssrl.68.3.386

Thingbaijam, K. K. S., & Mai, P. M. (2016). Evidence for truncated exponential probability distribution of earthquake slip. *Bulletin of the Seismological Society of America, 106*(4), 1802–1816. https://doi.org/10.1785/0120150291

Thøgersen, K., Sveinsson, H. A., Scheibert, J., Renard, F., & Malthe-Sørenssen, A. (2019). The moment duration scaling relation for slow rupture arises from transient rupture speeds. *Geophysical Research Letters, 46*(22), 12805–12814. https://doi.org/10.1029/2019GL084436

Tsai, V. C., & Hirth, G. (2020). Elastic impact consequences for high-frequency earthquake ground motion. *Geophysical Research Letters, 47*(5), 2019–086302. https://doi.org/10.1029/2019GL086302

Vanossi, A., Manini, N., Urbakh, M., Zapperi, S., & Tosatti, E. (2013). Modeling friction: From nanoscale to mesoscale. *Reviews of Modern Physics, 85*(2), 529–552. https://doi.org/10.1103/RevModPhys.85.529. arXiv:1112.3234.

Vargas, C. A., Basurto, E., Guzmán-Vargas, L., & Angulo-Brown, F. (2008). Sliding size distribution in a simple spring-block system with asperities. *Physica A: Statistical Mechanics and its Applications, 387*(13), 3137–3144. https://doi.org/10.1016/j.physa.2008.01.108

Velde, B., Dubois, J., Moore, D., & Touchard, G. (1991). Fractal patterns of fractures in granites. *Earth and Planetary Science Letters, 104*(1), 25–35. https://doi.org/10.1016/0012-821X(91)90234-9

Venegas-Aravena, P. (2023). Geological earthquake simulations generated by kinematic heterogeneous energy-based method: Self-arrested ruptures and asperity criterion. *Open Geosciences*. https://doi.org/10.1515/geo-2022-0522

Von Plato, J. (1991). Boltzmann's ergodic hypothesis. *Archive for History of Exact Sciences, 42*(1), 71–89. https://doi.org/10.1007/BF00384333

Wang, J.-H. (2019). A review on scaling of earthquake source spectra. *Surveys in Geophysics, 40*(2), 133–166. https://doi.org/10.1007/s10712-019-09512-4

Wojewoda, J., Stefański, A., Wiercigroch, M., & Kapitaniak, T. (2008). Hysteretic effects of dry friction: Modelling and experimental studies. *Philosophical Transactions of the Royal Society A: Mathematical, Physical and Engineering Sciences, 366*(1866), 747–765. https://doi.org/10.1098/rsta.2007.2125

Wu, Z. L., Chen, Y. T., & Kim, S. G. (1996). Physical significance of earthquake quanta. *Bulletin of the Seismological Society of America, 86*(5), 1623–1626.

Zang, A., & Stephansson, O. (2010). Rock fracture criteria. In: Zang, A., Stephansson, O. (Eds.) *Stress field of the Earth's crust* (pp. 37–62). Springer, Dordrecht . https://doi.org/10.1007/978-1-4020-8444-7_3

Zorzano, M. P., Mais, H., & Vazquez, L. (1999). Numerical solution of two dimensional Fokker—Planck equations. *Applied Mathematics and Computation, 98*(2), 109–117. https://doi.org/10.1016/S0096-3003(97)10161-8

(Received August 28, 2023, revised December 28, 2025, accepted January 21, 2026, Published online February 17, 2026)